Synthesis and Characterization of Nanocrystalline Transparent Conductive Oxides for Photocatalytic Applications

Daniela Filipa Claro Patrício

Thesis to obtain the Master of Science Degree in

Chemical Engineering

Supervisors: Prof. Dr. Alessandro Martucci

Prof. Dr. Ana Clara Lopes Marques

Examination Committee

Chairperson: Prof. Dr. Mário Nuno de Matos Sequeira Berberan e Santos

Supervisor: Prof. Dr. Ana Clara Lopes Marques

Members of Committee: Dr. António Cândido Lampreia Pereira Gonçalves

November 2019

This page was intentionally left in black.

UNIVERSITÀ DEGLI STUDI DI PADOVA

DIPARTIMENTO DI INGEGNERIA INDUSTRIALE

This work was developed in *Università degli Studi di Padova – Dipartimento di Ingegneria Industriale*, Padova, Italy.

This page was intentionally left in black.

I declare that this document is an original work of my own authorship and that it fulfils all the requirements of the Code of Conduct and Good Practices of the Universidade de Lisboa.

This page was intentionally left in black.

Acknowledgments

I would like to thank Prof. Alessandro Martucci, my supervisor in Italy, for giving me the opportunity to develop my dissertation at University of Padova and for helping me during my stay in his department and laboratory.

To my supervisor at IST, Prof. Ana Clara Marques, who supported me in the final period of this dissertation, thank you so much for all the availability and help on the data analysis.

I want to thank Nanomaterial Engineering Group, especially to Elena Colusso and Michele Rigon, for helping in all my work and problems, availability to answer my questions, and encouraging me to keep a positive attitude. To my colleagues, thank you for interacting with me and for the nice time spent on discovering Italian habits and music.

A big thanks to my family, without you nothing of this would be possible. For all my friends in Italy and Portugal who support me all the time, thank you.

This page was intentionally left in black.

Resumo

A presente dissertação tem como objetivo a síntese de filmes finos constituídos por óxidos condutores transparentes que possam ser simultaneamente aplicados como uma alternativa à utilização de óxido de índio dopado com estanho (ITO) e utilizados em aplicações de fotocatálise. Para tal, desenvolveram-se filmes de óxido de zinco (ZnO), ZnO dopado com Germânio (de acrónimo GeZO) e ZnO dopado com Silício (de acrónimo SiZO) através do método de Sol-Gel e *Spin-Coating*.

A estrutura cristalina dos filmes, a morfologia da superfície e as propriedades óticas e elétricas foram estudadas usando Difração de Raios-X, Microscopia Eletrónica de Varrimento (SEM), Elipsometria e Espectroscopia de UV-Vis, e a técnica de Quatro Pontas (*Four Probe)*, respetivamente.

Estudou-se a influência da concentração do precursor de zinco, a utilização de diferentes agentes de complexação, bem como o tempo de reação na preparação de filmes de ZnO. Concluiu-se que nenhum dos parâmetros afeta significativamente as propriedades estruturais dos mesmos.

Os filmes de GeZO produzidos com 2% molar de precursor de germânio exibiram cristalites bastante mais pequenas (5-7 nm) que os filmes de ZnO (15-20 nm). Quanto aos filmes de SiZO, estes exibiram uma diminuição dos parâmetros de rede e do tamanho das cristalites com o aumento da concentração, 1.5%, 3% e 6% molar, de precursor de silício. Tal facto deve-se à substituição de átomos de Zn por Si na rede, característico do processo de dopagem. Para ambos os filmes, a espessura dos mesmos aumenta com o número de camadas depositadas e não depende da concentração de dopante. Todos os filmes apresentam uma transmitância superior a 90% na zona do visível.

Os filmes produzidos possuem atividade fotocatalítica capaz de degradar uma tinta à base de 2,6-dicloroindofenol. Um dos filmes de GeZO e o filme de 3% SiZO possuem uma eficiência de cerca de 70% e 80%, respetivamente, ao fim de 5 minutos de exposição à radiação UV. Os valores obtidos são próximos do obtido para um filme de dióxido de titânio (TiO_2), habitualmente utilizado em fotocatálise (90%).

Palavras-chave: Filmes finos, ZnO, Ge dopante, Si dopante, Sol-Gel, fotocatálise

This page was intentionally left in black.

Abstract

The present dissertation has the objective of synthesizing transparent conductive oxides thin films, which can, simultaneously, be applied as an alternative to indium doped tin oxide (ITO) and used in photocatalytic applications. For that, zinc oxide (ZnO), germanium-doped ZnO (acronym GeZO), and Silicon-doped ZnO (acronym SiZO) films were developed by Sol-Gel Spin-Coating method.

The crystal structure, surface morphology, and the optical and electrical properties were studied using X-ray Diffractometer, Scanning Electron Microscopy (SEM), Ellipsometry and UV-VIS Spectroscopy, and Four Probe Technique, respectively.

The influence of the concentration of zinc precursor, the use of different chelating agents, and reaction time was studied in ZnO films preparation. All the parameters can achieve good film crystallization, without affecting the structural properties of the films.

The GeZO films with 2% mol of germanium precursor exhibited crystallites very smaller (5-7 nnm) than ZnO films (15-20 nm). The SiZO thin films exhibited a decrease of lattice parameters and crystallite size with the increases of concentration, of 1,5%, 3% and 6% molar, of silicon precursor. This is due to the replace of Zn atoms for Si atoms in the lattice. For both cases, the thickness increases with the number of layers and does not depend on dopant concentration. All films have a transmittance higher than 90% in the visible region.

GeZO and SiZO films exhibit photocatalytic activity, able to degrade a 2,6-dichloroindophenol-based ink. One of GeZO film and 3% SiZO film have an efficiency of 70% and 80%, respectively, after 5 minutes of UV radiation exposure. The obtained values are close to the efficiency of titanium dioxide film (TiO_2), usually applied in photocatalysis (90%).

Keywords: Thin films, ZnO, Ge doping, Si doping, Sol-Gel, photocatalysis

This page was intentionally left in black.

Development of TCO thin films by the Sol-Gel method

ZnO thin films

Evaluation of crucial parameters of the synthesis

Concentration

As made and ½

- Does not affect lattice parameters.

Decreasing the concentration:

- Crystallite size decreases slightly.
- Reduction in 60% in thickness, which could compromise electrical properties.
- Similar refractive index.

Chelating Agents

MEA or DEA

- Do not affect lattice parameters.
- Similar crystallite size.
- Same preferred orientation growth.
- MEA avoids higher nucleation barrier, promoting crystal growth along (002) plane.

Reaction Time

0.5, 1, 2, 4 or 7 h

- Good crystallization independently on reaction time.
- Similar thickness.
- Refractive index decreases slightly with the time but increases after 7h.

Conclusion

- The higher studied concentration to leads to good electrical properties.
- MEA promotes the growth in a specific plane.
- 0.5 h is enough to ensure ZnO formation.

GeZO thin films

Development of a new synthesis

Ge- and Zn- precursors in different starting solutions

- Polycrystalline films with ZnO formation.
- Decrease of crystallite size.
- Increase of lattice parameters.
- Presence of Zn_2GeO_4.

Conclusion

- Ge ions have lower radius than Zn ions, so lattice parameters must decrease.
- No evidence for a real doping of ZnO.

Ge- and Zn- precursors in same starting solution

- Ge-hydrolysis is very fast with high moisture, achieving turbid solutions.
- Acetylacetone does not change the hydrolysis rate.

2% Ge doping ZnO films with 2 or 3 layers (low humidity environment):

- Crystallite size decreases abruptly, which is useful for photocatalysis.
- Thickness and refractive index increase with the number of layers.
- Substrates have a huge influence on crystallization.
- Films have 90% of transmittance in Vis region.

SiZO thin films

Evaluation of crucial parameters of the synthesis

Addition of Water

With or without

- Crystallization in both synthesis.
- SEM pictures show dendritic structure for film with water (cracking).

Si-precursor

TEOS or $SiCl_4$

- Less crystallization for $SiCl_4$.

Thermal Annealing

H_2 or room atmosphere

- In H_2 atmosphere, samples were brownish and there is no formation of ZnO (presence of organic compounds).

Conclusion

To synthesize SiZO thin films without water and with TEOS as a Si-precursor. Annealing in room atmosphere and then in H_2 atmosphere.

1.5%, 3% and 6% Si doping ZnO films with 2 or 3 layers

- Lattice parameters decrease with the % of dopant.
- Crystallite size decreases with the Si-concentration due to the higher number of nucleation centers.
- Thickness increases with the number of layers and does not depend of Si-concentration.
- Films have 90% of transmittance in Vis region.

Photocatalytic Activity

- Substrate, GeZO and SiZO exhibit photocatalytic activity.
- One sample of GeZO and 3% SiZO have a similar behavior than TiO_2, a well-known catalyst semiconductor.
- Used method have some limitations due to the spot of incident UV light.

This page was intentionally left in black.

Contents

List of Figures

List of Tables

This page was intentionally left in black.

Nomenclature

CBM – Conduction Band Minimum

DEA – Diethanolamine

EtOH – Ethanol

FTIR – Fourier-transform Infrared Spectroscopy

FWHM – Full Width at Half Maximum

GeZO – Ge-doped zinc oxide

IPA – 2-propanol or isopropanol

ITO – Tin-doped indium oxide

MEA – Monoethanolamine

SEM – Scanning Electron Microscopy

SiZO – Si-doped zinc oxide

TCO – Transparent Conductive Oxides

TEOS – Tetraethyl Orthosilicate

VBM – Valence Band Maximum

XRD – X-Ray Diffraction

ZnAc – Zinc acetate dihydrate

ZnO – Zinc oxide

This page was intentionally left in black.

1. Introduction

1.1. Context

Transparent Conducting Oxides (TCOs) are materials that exhibit high optical transmittance in the visible range and electrical conductivity close to that of metals [1]. This unusual combination of properties makes TCO a widely applied component in many areas, such as optoelectronic devices, gas sensing, and solar control.

During the last years, the electronics market is growing fast, and the demand for these materials is extensively increased. Therefore, issues with a stable supply of tin-doped indium oxide (ITO), the most popular used TCO, began to appear. Indium is scarce and only can be produced as a by-product with very high costs [2,3]. As a result, investigating and developing an alternative TCO is extremely necessary to achieve the same specificities through more earth-abundant materials at a lower cost [4].

In recent years, studies with Zinc Oxide (ZnO) demonstrated that this material is a promising alternative to ITO. Zinc is more abundant than Indium, is low-cost, and non-toxic [3,5]. Moreover, ZnO has wide band gap energy and high electron effective mass, which allows having high optical transmittance [6,7].

Despite presenting many advantages, ZnO shows a relatively high resistivity, and consequently, a low conductivity, which could be a problem for several applications [5]. Indeed, the combination of both optical and electrical properties is only possible by introducing appropriate dopants in the ZnO crystal lattice to replace Zn [8]. Doping with impurities, it is possible to improve the electrical properties without degrading the optical transmittance. [1] However, one of the critical challenges is to understand what the best dopants and optimal contents are.

To choose an adequate dopant, it is important to consider two different criteria: electronegativity and ionic radius. The ion dopant, which will substitute the Zn^{2+}, must have a higher valence to increase the number of free electrons. On the other hand, the dopant should have a similar radius to zinc ion so it cannot provide a significant lattice distortion. Nevertheless, its selection should have into account the final application for which it is intended.

In doping ZnO, germanium (Ge)- and silicon (Si)- ions can be used to substitute the host atom in the lattice [9]. These non-metallic elements belong to group IV, so they have four free electrons and, therefore, act as two-electron donors, which contribute to the electric conductivity. Furthermore, Ge^{4+} and Si^{4+} have radii of 0.053 nm and 0.041 nm, respectively, that are similar to Zn^{2+} radius (0.074 nm).

ZnO and doped-ZnO have also been considered as a substituent of titanium dioxide (TiO_2) for photocatalytic applications. ZnO has ideal optoelectronic, catalytic, and photochemical properties, together with a lower Band Gap than TiO_2, which provides a better photocatalytic activity under visible light illumination. Moreover, the degenerated holes in ZnO have strong enough oxidizing power to decompose most organic compounds, such as aqueous solutions of several dyes and other

environmental pollutants [10]. For this reason, ZnO could have a crucial role in mitigating environmental pollution and being a renewable and sustainable energy source.

According to this context, the present Master Thesis in Chemical Engineering was developed with the main objective of synthesizing Ge- and Si-doped ZnO-based TCOs. These oxides should exhibit adequate electrical and optical properties to substitute ITO in its applications and to allow their use in photocatalytic activities.

1.2. Objectives

The main objective of this work is to develop TCOs thin films alternative to the most used ITO from liquid solutions. To obtain functional thin films, Ge-doped ZnO (GeZO) and Si-doped ZnO (SiZO) solutions are developed by the Sol-Gel method and, posteriorly, deposited on silicon or fused silica substrates by Spin-Coating and annealed by Heat Treatment.

As-prepared films are characterized to study their structural, optical, and electrical properties and assess their use as ITO substitute and for photocatalytic applications.

1.3. Structure

This dissertation is divided into five chapters which have the following structure:

Chapter 1 – It includes the framework of the thesis, with the main objectives and its structure.

Chapter 2 – This chapter englobes the State of the Art and some definitions and essential concepts.

Chapter 3 –Englobes the experimental procedures to developing different TCOs, their characterization with different methods and respective results and discussion.

Chapter 4 – It includes the application of TCOs for photocatalytic activities.

Chapter 5 – The last section includes a brief conclusion and future work.

2. Overview

2.1 Transparent Conductive Oxides

Transparent Conductive Oxides are semiconductors with a non-metal part, consisting on oxygen, and a metal part. The metal or metal-combination allows these materials to have different optoelectrical properties, which can be changed by doping with metals, metalloids, or non-metals [11].

The first TCO material was reported in 1907 when Bädeker observed the electrical conduction and transparent properties of cadmium oxide (CdO) thin film by thermal oxidation of sputtered cadmium [12]. After the Second World War, the electronics market grew, and many binary oxides systems with good transparent conducting properties were discovered. For example, tin (II) oxide (SnO_2)-based transparent coating was proposed for de-icing airplanes windows at high altitudes, while ZnO was investigated for surface acoustic wave devices, due to its piezoelectric properties [13,14].

At the end of the 1960s, scientists used filters of SnO_2 and indium oxide (In_2O_3) to improve the sodium discharge lamps efficiency, reducing heat losses. Since this discovery, ITO was widely applied for transparent electrodes and remained the primary choice for the current industries, because it has superior electrical and optical properties [7,15].

In the decades that followed, new TCO materials were extensively studied to obtain TCO films for specialized applications. In the 1990s, studies to develop multicomponent oxide-based TCO were made, combining binary oxides, such as ZnO, CdO, In_2O_3, and SnO_2. For instance, to change the electrical, optical, chemical, and physical properties of ternary compounds made possible their use for new applications [9].

Until now, many researchers dedicated a lot of time to study ZnO to improve its properties using new dopants and allowing its use for all the ITO applications. However, these are empirical-based studies, due to the doping mechanism is not clear yet for crystalline ZnO and other TCO materials [5].

2.1.1. Electrical and optical properties

There are several properties required for a TCO to achieve optimal performance. For a better understanding of the electrical and optical properties of TCOs, we must look at the semiconductors class.

The Semiconductor Band Theory explains the presence of electrical properties in solids. During the formation of a solid compound, the interaction between bonding and antibonding combinations of atomic into molecular orbitals results in discrete and close energy levels that constitute a continuous band. So, a band is a series of possible energy levels for electrons [16, 17]. The energy level corresponding to the highest occupied molecular orbital is called Valence Band Maximum (VBM), while the lowest unoccupied molecular orbital is referred to as the Conduction Band Minimum (CBM) [16]. The energy difference between these two bands is the Band Gap Energy.

According to the theory and based on conductivity, there are three categories of materials – conductors, semiconductors, and insulators. In a semiconductor material, the valence band is filled and the energy band gap is low enough to permit electronic changes. By thermal or photonic excitation, the ground state electrons are excited to the conduction band, occupying a high level of energy and allowing the electrical conduction. This event creates holes in the valence band that are occupied for electrons from a lower level of energy, which creates new holes, and like this successively. For this reason, the charge carriers are electrons (n) and holes (p).

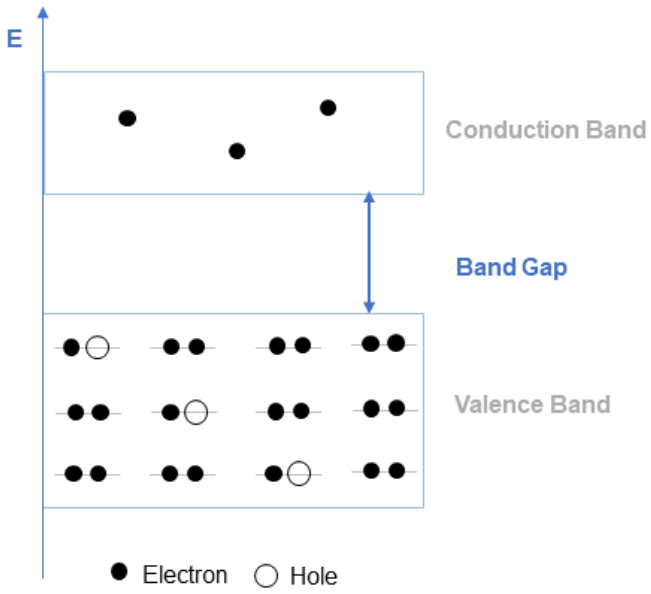

Figure 1 *– Schematic representation of conduction in a semiconductor. Adapted from [17].*

It is possible to identify two types of TCO semiconductors – intrinsic and extrinsic. The first one corresponds to the pure form of semiconductors, while the second one exhibits conductive properties due to the intentional introduction of impurities or defect sites in the crystalline network or the formation of non-stoichiometric oxides. Without doping, TCOs like ZnO, In_2O_3, CdO, and SnO_2 would be transparent insulators [1].

When the introduced impurity is an atom of an element with higher valence than the standard atoms in the structure, there are one or more electrons that are weakly connected. They are located in supplementary levels of energy, immediately under the CBM. A small amount of energy is enough to promote their passage to the conduction band and the substance becomes conductive. The conduction is due to the electrons and the material is an n-type semiconductor ($n > p$). On the other hand, if the new element has a lower valence, it is not possible all atoms do all connections, which creates holes in the lattice. In this case, the conductivity is related to the holes and the material is a p-type semiconductor ($p > n$).

The electrical conductivity of ZnO, as an n-type semiconductor, is primarily dominated by electrons generated by oxygen vacancies and charge donation [3].

The conductivity (σ) of n-type materials is given by the density of charge carriers in the conduction band and their mobility within the crystal lattice [7,8].

$$\sigma\ (S \cdot cm^{-1}) = n \cdot e\ \cdot \mu \tag{1}$$

Where n is the density of free electrons (cm^{-3}), e is the electronic charge (C) and μ is the electron mobility ($cm^2(V \cdot s)^{-1}$).

In its turn, the mobility is related to the effective electron mass (m_e) and the scattering time (τ) which results in the sum of scattering due to impurities, defects, and grain boundaries – equation (2).

$$\mu = \frac{e.\tau}{m_e} \tag{2}$$

The electrical conductivity is intrinsically limited because n and μ cannot be independently increased for practical TCOs. Increasing dopant concentration, the density of charge carriers increases, but the carrier transport is limited by ionized impurities scattering. On the other hand, this increase reduces the mobility to a level that conductivity remains constant and reduces the optical transmission. Besides this, a high concentration of dopants could form ion clusters, which increases the scattering rate [18].

Another important parameter is the resistivity (ρ), which is the inverse of the conductivity. Measuring experimentally the sheet resistance, it is possible to predict the resistivity, and, consequently, the electrical conductivity.

$$\rho\ (\Omega \cdot cm) = \frac{1}{\sigma} \tag{3}$$

Electrical and optical properties are intimately related. To understand the optical properties in TCO materials, it is essential to distinguish the difference between fundamental Band Gap, as described above, and Optical Band Gap, which corresponds to the smallest allowed optical transition from the Valence Band (VB) to Conduction Band (CB). According to the Band Theory, the introduction of defects in a metal oxide can create an excess of electrons close to the defect sites. If there is orbital overlap enough, electrons could be delocalized, and CBM becomes filled – Moss-Burstein Effect [7,16]. For this reason, the Optical Band Gap is the sum of Band Gap and the Moss-Burstein shift (4).

$$E_g^{opt} = E_g + E_g^{MB} \tag{4}$$

Additionally, the separation between the higher level of CB and the next electronic energy level (CBM+1) must be higher than 3,1 eV to prevent unwanted optical absorption and, consequently, to provide transparency in the visible spectrum [16].

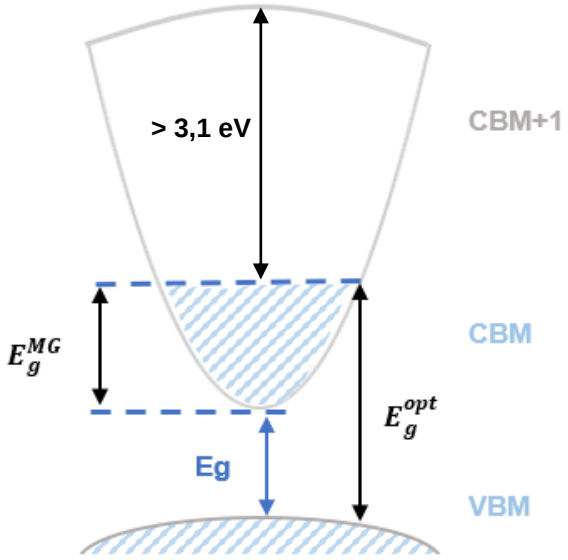

Figure 2 *– Diagram of the Moss-Burstein Effect and Optical Band Gap. Adapted from [16].*

Apart of Moss-Burstein Effect, the Band Gap is reduced due to the Band Gap Narrowing effect, which led by exchange interactions in the free electron gas and electrostatic interactions between free electrons and ionized impurities [3].

Besides high conductivity, effective TCO thin film should have a very low absorption coefficient in the near UV-Vis-NIR region. Analyzing a typical transmission spectrum of a TCO, it is possible to identify three main areas (Figure 3). In the visible region, typically defined as a wavelength (λ) between 400-750 nm, TCOs must be transparent. In the near UV (< 350 nm), the transmission decreases abruptly, due to the absorption of light with energy above the Band Gap Energy (around 3,1 eV). For higher wavelengths (> 1500 nm), in the IR region, the frequency of the light is the same as the frequency of the oscillation of electrons, which results in a minimum of transmission, corresponding to plasma wavelength [19].

The optical properties of TCOs, transmission (T), absorption (A), and reflection (R), are determined by its refraction index n, extinction coefficient k, Band Gap, and geometry. In its turn, geometry is an extrinsic property that englobes the film thickness, thickness uniformity, and film roughness, which influence the sheet resistance.

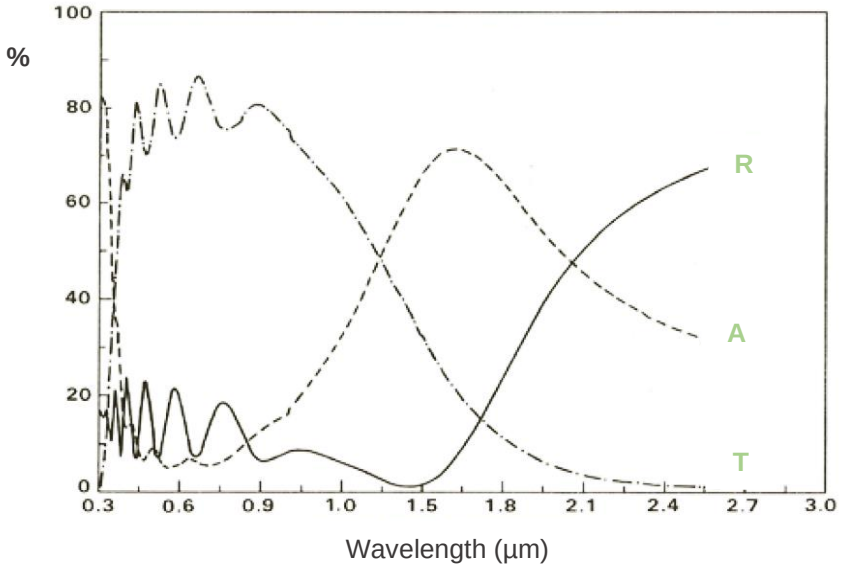

Figure 3 *–Typical transmission, reflection, and absorption spectra of a TCO. Adapted from [TCO15].*

The development of TCO must represent a compromise between electrical conductivity and optical transmittance [20]. The best way to improve the conductivity without degrading significantly the optical properties is to increase the mobility, instead of the carrier concentration, which is inversely related to plasma wavelength.

2.1.2. Development of TCO materials

Several elements are doped ZnO films, mainly elements from group 13, such as Al, Ga, In and group 16, like F. Among them, the most studied are Al-doped ZnO and Ga-doped ZnO. Nevertheless, using elements of group 14, like Ge and Si, it is expected that they act as a two-electron donor, which can generate higher free carrier concentration and, consequently, increase the conductivity [21].

Additionally, Ge and Si are semiconductors with smaller effective masses for electron-hole pairs (excitons), a narrow Band Gap, and high carrier mobilities with a large absorption coefficient [22]. Due to these all characteristics, it is expectable that it is easier to change the electronic structure around the band edge [23].

The study of Ge-doped ZnO has been done applying different techniques, such as Solid-State Reaction, RF Magnetron Sputtering, and Pulsed Laser Deposition. Using the first method at 600°C for 6 hours, it was discovered that Zn_2GeO_4 phases are formed by the heavy doping of Ge atoms [24].

In thin films prepared by RF Magnetron Sputtering, was observed resistivity as $2 \times 10^{-3}\ \Omega \cdot cm$ and, for higher conductive films, the absorption near the visible region decreases slightly [25]. Another study reports the formation of Zn_2GeO_4 and the decrease of crystallization of ZnO due to the defects associated with the incorporation of Ge atoms [26].

ZnO films prepared by the Sol-Gel method and doped by ion implantation show a higher optical band gap, comparing with undoped films [23]. Using Atomic Laser Deposition at 250°C and Tetramethoxygermanium (IV) as a precursor, it was possible to obtain mobility as $5\ cm^2 \cdot V^{-1} \cdot s^{-1}$ [27]. In its turn, using Pulsed Laser Deposition at 300°C and several pressures, it was concluded that the minimum value of resistivity is $6{,}5 \times 10^{-4}\ \Omega \cdot cm$ for 10 mTorr with a transmittance above 80% [28].

A theoretical study reported the tendency of Ge atoms to form clusters that can limit the conductivity but reinforce the near-band-edge emission. It also shows a stronger Ge-O bond than Zn-O bond. More recently, the formation of nanoparticles of Ge was studied using Solution-Phase Synthesis and Colloidal Synthesis. The effort here is to understand the morphology of nanocrystals and the structure of films with or without reducing agents [22,29,30].

Like happens with Ge, also several methods have been used to study the behavior of Si-doped ZnO. The first reported research using RF Magnetron Sputtering includes the development of films deposited using temperature below 250°C with resistivity as low as $3{,}8 \times 10^{-4}\ \Omega \cdot cm$ and transmittance above 85% in the visible range [31]. Recently, films with resistivity as $4{,}9 \times 10^{-4}\ \Omega \cdot cm$ and transmittance above 90% using the same approach was reported [32].

Using Pulsed Laser Deposition, SiZO thin films deposited on sapphire substrates and grown at 600°C exhibit resistivity as $6{,}2 \times 10^{-4}\ \Omega \cdot cm$ and a Band Gap upper than undoped ZnO [33]. Another research group reported films deposited at 100°C, resulting in resistivity as $7{,}9 \times 10^{-4}\ \Omega \cdot cm$. They also observed a strong dependence of electronic properties and substrate nature [34].

The use of Fluoride in Spray Pyrolysis for SiZO solutions decreased the electrical resistivity to $1{,}5 \times 10^{-3}\ \Omega \cdot cm$ and allow transmittance of 87% [35]. Other article reported a resistivity as $3{,}7 \times 10^{-3}\ \Omega \cdot cm$ [36]. The optical and structural properties after heat treatment at 550°C were studied using Sol-Gel Spin-Coating method. However, no electrical resistivity data were reported [34].

Analyzing the above information, it is possible to observe that studies of GeZO and SiZO were not made extensively and, due to this, the information about fundamental factors that determine the doping composition and the dependence of optoelectronic properties is still limited [21,28]. To notice, however, that the values of resistivity and mobility for undoped and doped-ZnO do not change substantially. It means that probably exists a physical limit, preventing obtaining resistances below $10^{-4}\ \Omega \cdot cm$ and mobilities above $40\ cm^2 \cdot V^{-1} \cdot s^{-1}$ [5].

2.1.3. Applications

TCOs have several applications used in aerospace, architectural, solar energy, and electronics industries [15]. It is important to refer that ZnO is investigated as a substituent of ITO, but due to its non-optimal electrical and optical properties, it cannot be applied yet in some areas on an industrial scale. According to the developed experimental work made in this dissertation, photocatalytic applications will be described with more emphasis.

The photocatalysis process is an advanced oxidation process that can remove, eliminate or degrade hazardous materials, bacteria, and organic and pharmaceutical pollutants by photodegradation [1,37]. Due to its characteristics, it is a technique with significant potential for environmental conservation, such as wastewater treatment and waste treatment with green energy production, and for self-cleaning surfaces. In this process, the reactions are initialized when semiconductor absorbs photons with higher energy than its Band Gap. It promotes the transition of induced electrons from the VB into the CB, leaving a hole behind. A fraction of photoexcited excitons diffuses to the surface of the catalytic particle and can take part in chemical reactions with the adsorbed donor (D) or acceptor (A) molecules [38].

The holes can react with water molecules/OH^- ions to induce the formation of reactive species, such as OH radicals, with strong oxidizing function. On the other hand, atmospheric oxygen (O_2) acts as an electron acceptor and forms a superoxide ion - $O_2^{\bullet -}$. The presence of these species facilitates the degradation of organic pollutant molecules [39].

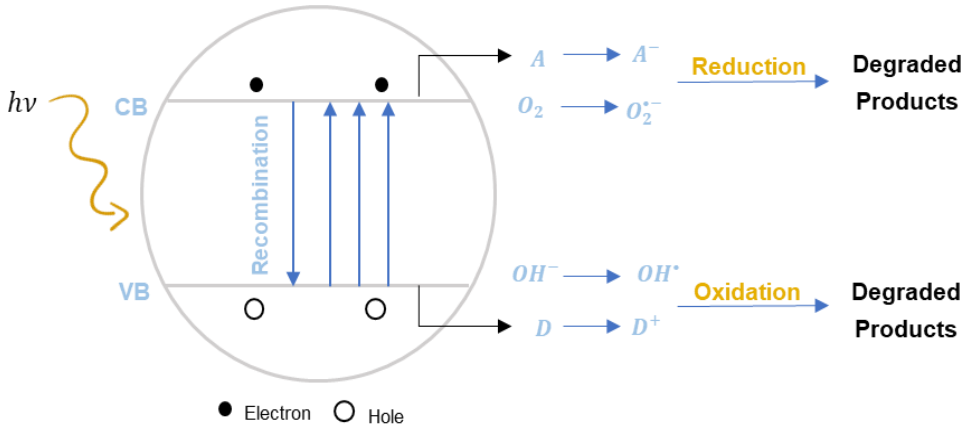

Figure 4 *– Schematic Mechanism of a typical Photocatalysis in a TCO semiconductor. Adapted from [40].*

In any photocatalytic process, the exciton generation via the transition of electron between VB and CB is fundamental, and its charge carriers are the main role in this process [41]. However, the photocatalytic activity of ZnO is hampered due to the fast recombination of photo-generated holes in VB with the photo-excited electrons in CB [37]. Doping is one of the best solutions to improve its photocatalytic properties because it can modify the Band Gap and introduce charge traps, suppressing the charge carrier recombination [37].

There are several factors to take into account to enhance the performance of the photocatalytic activity. An important parameter is the surface area and morphology of the film. Reducing the crystallite size, the active surface area in contact with the pollutant is higher, improving the photocatalytic properties. If catalyst concentration is excessive, the photonic efficiency will become smaller, and the semiconductor surface will become saturated, decreasing the rate of reaction. On the other hand, increasing the initial concentration of pollutants, the organic compounds adsorbed on the surface is higher, and the photocatalyst efficiency reduces [42].

Another crucial parameter is the incident Light Intensity [43]. With higher intensity, it is possible to eliminate the recombination process, enhancing the photocatalytic activity. Moreover, high UV absorption is needed to introduce as many photons as possible into the film, making critical the adjustment of intensity to the semiconductor Band Gap. However, if the film is too thin, UV radiation will penetrate it and may damage other parts of the structure [38].

In Solar Control, Low-emissivity glass is the most significant marketed window treatment. It promotes a good light transmission in the visible range, minimizing heat transfer. In heat-efficient window applications, the TCO is used as a filter that reflects in the UV while remaining transparent in the visible region. In buildings with these windows, it is possible to minimize the costs of heating in cold climates, while in hot environments the opposite approach is taken [1,15]. This glass is very cost-effective when compared with double glazing and can reduce heat loss by over 70% [44].

Gas Sensor implementation is crucial to detect and to monitor toxic gases in domestic and industrial environments. A gas sensor is designed to convert chemical information (concentration) of a specific gas into an electric or optical signal [45]. The gas recognition is made by adsorption, reduction, or electrochemical reactions for the receptors, and the surface conductivity is monitored. The surface captures oxygen from the air, which is converted into oxygen ions by taking electrons from the conduction band, decreasing the conductivity.

TCO coatings are used as defrosters in aircraft windshields. Applying electrical current, the layer is heated and prevents the air condensation [46]. It needs a reduced effective defroster time than traditional hot air blowers and covered uniformly large areas. However, their implementation for passenger vehicles is not possible yet, due to the high cost of a new alternator with adequate voltage [8].

Additionally, TCO coatings can be applied as shielding to decrease electromagnetic radiation interference and to provide visual access. One of the prominent examples is the microwave oven window because they allow transparency and minimize the microwave leakage. On the other hand, they can be used for antireflection coatings for antiglare purposes, offering an antistatic function [15].

Despite a vast world of optoelectronic applications, the TCOs thin films are used predominantly for Flat Panel Displays (LCDs) and Solar Cells. In the first one, TCO films are used in a standard electrode layer, allowing maintenance of a uniform pixel voltage across the whole LCD screen when the backlight passes through the liquid crystal film [8]. For Solar Cells, TCO material must have high conductivity and transparency, large area capability, low cost, and stability under environmental conditions [46]. In both cases, ITO is the best choice.

The TCO materials are usually n-type semiconductors, but recent research has studied the p-type semiconductors for solid lasers. However, due to their difficulty in obtaining these materials, they have not yet an industrial application.

2.2 TCO thin films formation

ZnO thin films have been prepared by different methods, including Physical Vapor Deposition and Chemical Solution Deposition processes [47]. Physical depositions always take place under vacuum or a controlled atmosphere and include methods like Sputtering, Magnetron Sputtering, and Pulsed Laser Deposition. On the other hand, Chemical Deposition is a simple and low-cost alternative that provides a large-area thin film. Examples of this are Spray Pyrolysis, Electrodeposition, and Sol-Gel method [48].

Among all the above approaches, Sol-Gel is one of the most popular routes for oxide materials synthesis. Indeed, it is predominantly advantageous, because it includes process simplicity, requires only small amounts of precursors, does not involve high temperatures and provides easy control over film composition and uniformity of its thickness [47,49,50].

It is important to refer that the used technique influences the properties of the films. Even if different workers use the same method and the experimental conditions were very close, it is possible to obtain different results, mainly concerning the crystallographic orientation. This makes difficult to predict any results and to do correlations [51]. Therefore, the effect of preparation conditions on the properties must be considered for its practical technological applications.

2.2.1 Sol-Gel technique

Sol-Gel chemistry involves a series of hydrolysis and condensation reactions of the precursors in acid or basic aqueous or alcohol solution, forming colloidal particles controllably aggregating into a wet network [19].

It is possible to identify several steps in Sol-Gel method:

(i) formation of a colloidal suspension of solid particles via hydrolysis and partial condensation of precursors (sol);
(ii) gelation resulting from colloidal particles bonding which formed a three-dimensional and interconnected oxide network enclosing a continuous liquid phase [52];
(iii) aging and drying of the gel with the collapse of the porous network caused by solvent and water evaporation;
(iv) thermal decomposition of the gel at high temperature [53].

A general scheme to prepare a film is shown in Figure 5. During the sol step, precursors are hydrolyzed and partially condensed. After the deposition on the substrate by the chosen technique, gelation and evaporation of the solvent occur and, after the heat treatment, it is possible to obtain a functional and stable film [51]. Depending on the specific application, the different stages can be extended and altered.

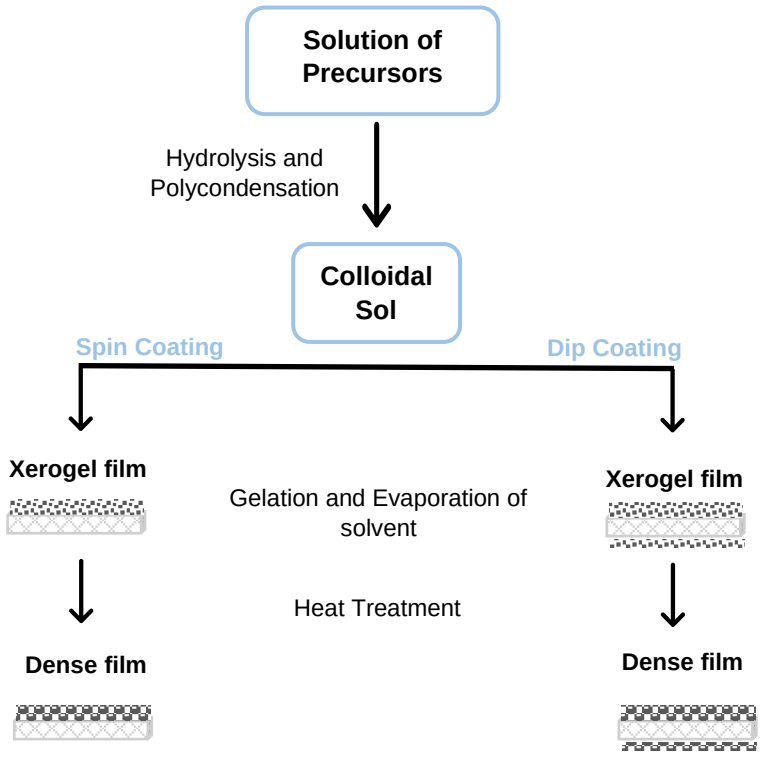

Figure 5 *– Schematic representation of Sol-Gel process for films from a colloidal sol. Adapted from [51].*

Two Sol-Gel routes are currently used, depending on the nature of the molecular precursors: metal alkoxides in organic solvents or metal salts in aqueous solutions [54]. Nowadays, the principal method to synthesize ZnO films is an intermediate technique, which uses zinc metal salts in an alcoholic solution. Using metal alkoxides as a precursor reveals some complications in process and product control, due to its moisture sensitivity and its rapid reaction rate. Moreover, it is too expensive for some applications [55,56]. Metal salts are a good alternative because of their low cost and their better results for large-scale applications. Inorganic metal salts like nitrates, chlorides, and perchlorates are often used, but they require relatively high temperatures (100-200°C) to induce hydrolytic reactions and it is difficult to remove anionic species in the final product [57]. The use of organic metal salts, such as acetates, remains the best solution. Acetate groups decompose under annealing which allows their elimination as volatile by-products [51].

The solvent must have a relatively high dielectric constant to allow the metal salts dissolution. Alcohols with low carbon number up to four are commonly used: methanol, ethanol, 1-propanol, 2-propanol, 1-butanol, and 2-methoxyethanol. Ethylene glycol has also described as a solvent [58]. Among all the alcohols, the most used are ethanol and 2-propanol. Indeed, methanol and 2-methoxyethanol present good chemical properties, but they are toxic.

A stabilizing agent is added to promote a complete dissolution of the precursor into the solvent. This type of additive plays an essential role as a chelating agent and stabilizing ligands, which avoids the premature precipitation and inhibiting the rapid conversion of the sol into a gel [58]. Alkali metal hydroxides, carboxylic acids, alkanolamines, alkylamines, acetylacetone, and polyalcohols are

frequently used for this purpose. In the specific case of the use of amines, these can increase the pH of the solution, which should promote the formation of ZnO [51].

After hydrolysis and partial condensation reactions, it is possible to deposit the solution onto the substrate. The added value of Sol-Gel comes from the possibility of employing the homogenous solution that was obtained before the gelation to prepare thin films using spin or dip coating [53]. Therefore, the crucial parameter is the aging time, which must be short to avoid the gel formation, but enough to allow hydrolysis reactions occur extensively.

The control of concentration and type of precursor, solvent, and additives, as well as solution pH and aging time, play an important role in the crystallization and texture of the films. Moreover, to obtain functional films, it is crucial to control the method of coating of substrates and its speed, the nature of the substrate, and the pre- and post-heat treatment.

2.2.2 Deposition and treatments

To obtain homogenous and uniform coating on different substrates, the sol solution can be deposited through various techniques, such as spin coating, spray coating, and dip coating. Spin-coating is currently the most used technique to produce thin films with a thickness of the order of micrometers and nanometers in laboratory conditions and for small and regular shape samples [59]. Its main advantages are easy control and repeatability capacity, which allows the fabrication of thin films at faster rates with desire morphologies and properties [60].

Spin-coating can be divided into four key stages: (i) deposition, (ii) spin-on, (iii) spin-off, and (iv) evaporation. However, evaporation normally overlaps the other stages. During the deposition stage, an excess of solution is deposited on the surface of the substrate. In the spin-on stage, the liquid flows radially outward, driven by centrifugal force [59]. The acceleration causes a spiral vortex in the solution with the expulsion of most of the liquid. At the end of the acceleration ramp, the speed remains constant [19]. In the spin-off stage, excess of liquid flows to the edge and leaves as droplets. As the film thins, there is greater resistance to flows, and consequently, the rate of removal of excess liquid decreases. This can be justified by the increase of the concentration of the non-volatile components, which raises the viscosity [50]. In the last stage, the residual solvent is eliminated by evaporation.

Due to the balance between centrifugal force, which drives flow radially outward, and viscous force, which acts radially inward, the film becomes uniform in thickness during spin-off and, since uniform tends to remain so [61].

The thickness and uniformity of the final product are affected by the rheological characteristics of the solution, and by spinning parameters (spin speed, time of spin, acceleration, atmosphere of deposition) [60]. The substrate also has an important role in obtaining uniform films. Thus, before the solution deposition, it must be clean to avoid the presence of contaminants, which could affect the thin film quality and its adherence on the substrate.

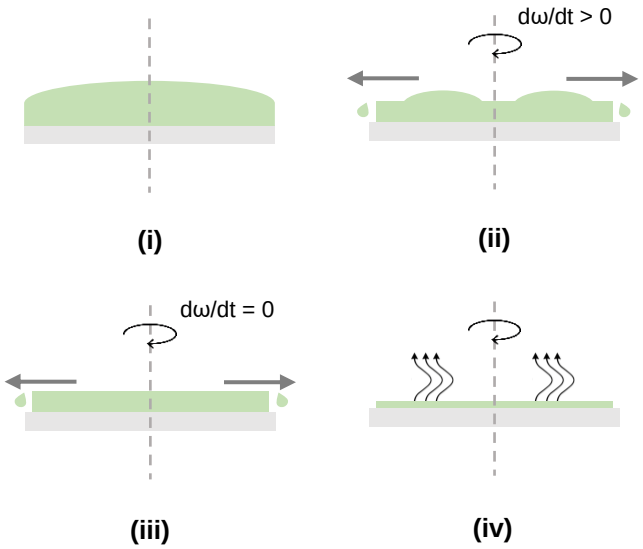

Figure 6 *– Four stages of spin coating. (i) deposition; (ii) spin-on; (iii) spin-off; (iv) evaporation. Adapted from [60].*

Several layer depositions must be made to obtain the desired thickness. After each layer, a pre-heat treatment is required to guarantee the total evaporation of organic species and to induce the formation and crystallization of ZnO. The chosen temperature must be high enough to allow the thermal decomposition of all compounds.

Finally, the deposited film is annealed at a high temperature. Annealing is a post-heat treatment that involves heating the material to above its critical temperature, maintaining a suitable temperature and then cooling. It can enhance structure homogeneity, relieve internal stresses, which promotes the formation of Zn-O bonds in the ZnO thin film [62]. Moreover, the dopant diffuses into the ZnO structure in this stage.

After the post-treatment of doped ZnO thin films, it is observed an improvement in the film transparency, resulting from the increased crystallinity and the reduced surface roughness. Indeed, as the grain size increases, the boundary scattering tends to decrease, affecting the transmittance favorably. Under a reducing atmosphere, the Optical Band Gap is widened, and the electrical properties are improved, due to the passivation of grain boundaries and zinc ions, which increases carrier concentration and mobility [7].

2.2.3 Sol-Gel reactional mechanism

Zinc acetate dihydrate ($Zn(CH_3COO)_2 \cdot 2H_2O$, ZnAc) was used as a starting compound. This choice was made considering that acetic acid, one of the products of the hydrolysis reaction, is very soluble in the solvent medium [56].

In the alcoholic solution, the precursor dissociates into zinc monoacetate and acetate ions, as shown in equation (5).

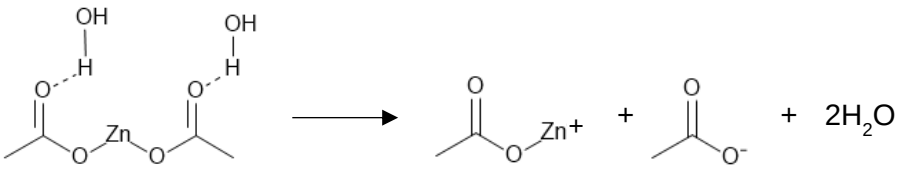

(5)

During the deposition, the formed ions and water are adsorbed on the substrate, and the zinc acetate is hydrolyzed, giving rise to zinc hydroxide and acetic acid [63]. The temperature of drying process must be higher than to the boiling point of acetic acid to allow its evaporation (equation (7)).

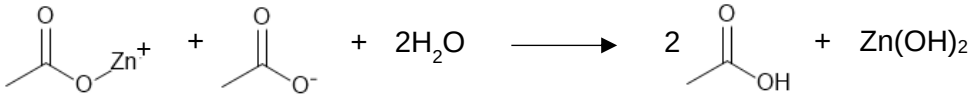

(6)

(7)

However, in the presence of hydroxyl groups, the condensation extension is lower, leaving intermediate products in the film. On the other hand, if the precursor concentration is high, there is not enough time to react completely in sol step, which provides incomplete hydrolysis and condensation too.

It is known that condensation is favored by alkaline conditions, which are provided by the addition of monoethanolamine (MEA) or diethanolamine (DEA) [63]. Indeed, they help the dissolution of zinc acetate in an alcohol medium, and, consequently, promote the bridging between two zinc atoms [63]. As a result, the formed zinc acetate can interact with the amine group of MEA/DEA, favoring the hydrolysis and polycondensation reactions of zinc species. In the following equations, it is possible to observe the mechanism with DEA (equations (8-10). On the other hand, the amine compound can react with zinc acetate via the hydroxyl group, which can result in by-products (equation (11)). [64]

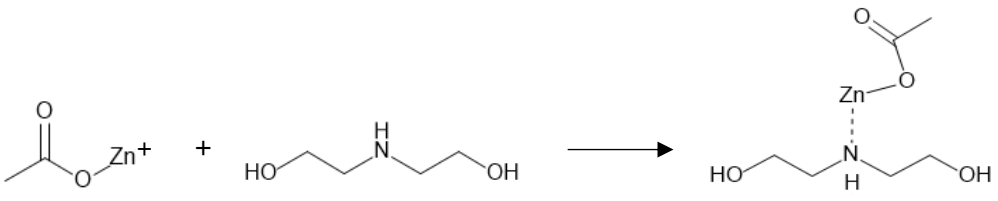

(8)

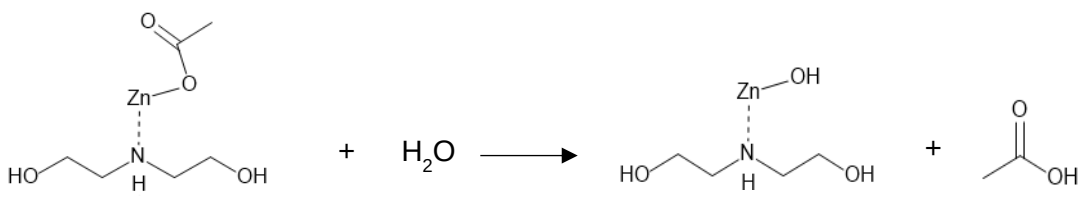

(9)

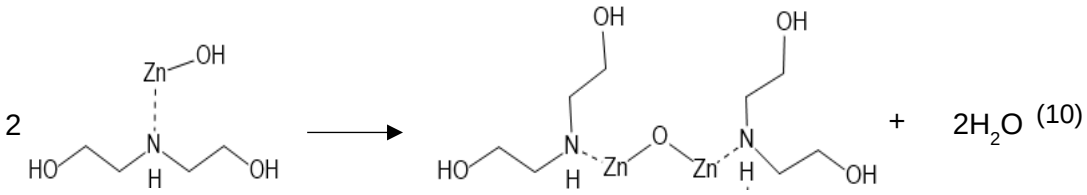

(10)

(11)

Finally, when the reactions continue, another oligomer of Zn-O-Zn is formed. The resultants of the reaction when heated were transformed into ZnO [65].

3. Synthesis and characterization of thin films

All the thin films were synthesized using Sol-Gel Spin Coating and deposited onto silicon or fused silica substrates. The substrates were cleaned using a basic piranha solution at 60°C for 20 minutes, with hydrogen peroxide (30% wt. solution), ammonia (25% wt. solution), and deionized water, according to 1:3:5-10 volume ratio. This procedure allows to remove residual organic compounds and impurities. After a carefully clean with deionized water, the substrates were stored in water, and, before the deposition process, they were dried with an air stream.

Films characterization was made using different methods. Their structure and orientation were analyzed by X-ray Diffraction (XRD), while the thickness and the refractive index were determined by Spectroscopic Ellipsometry. Scanning Electron Microscopy (SEM) allowed observation of film surface morphology. The electrical properties were measured using the 4-Probes Technique, and optical properties were obtained by UV-Vis Spectroscopy. A brief description of them is presented in Appendix A.

3.1. Synthesis of TCOs

3.1.1. ZnO thin films

The synthesis of functional ZnO thin films englobes several parameters that influence the final result, as described in Chapter 2. Different Sol-Gel routes are reported in the literature, and, as a first approach, the synthesis developed by Nanomaterial Engineering Group of the University of Padova was used [66]. The main objectives are to study three crucial factors – Zinc precursor concentration, effect of different chelating agents and reaction time – and to develop the final recipe with all the parameters optimized.

The initial procedure involved 200 mg of Zinc Acetate Dihydrate (ZnAc) dissolved in 0.9 mL of ethanol (EtOH). Then 0.066 mL monoethanolamine (MEA) was added under stirring at 60ºC to provide a transparent solution. After 30 minutes, 0.35 mL of EtOH was added, and the solution was deposited on the substrate after more 5 minutes of stirring.

To understand the role of Zinc precursor concentration, two solutions were prepared. The second solution has a half concentration of the first one. They were deposited onto silicon substrates by spin coating at a speed of 2000 rpm for 30 seconds. A pre-treatment was performed at 300ºC between each layer to evaporate organic compounds. The layer deposition cycle was repeated two times. Finally, a post-treatment was made at 500ºC with a ramp of 5°C/min, during 1 hour.

The previously reported synthesis was again reproduced to evaluate the effect of different stabilizers, substituting MEA for DEA. The molar ratio of DEA to ZnAc was maintaining at 1 [4].

The reaction time is not well defined in the literature and can vary between 30 minutes and several hours [5,20,66]. For this reason, five solutions with different condensation times were reproduced using the first synthesis with MEA.

3.1.2. GeZO thin films

The synthesis of Ge-doped ZnO thin films is not reported yet in the literature. As an initial approach, the procedure developed for ZnO thin films was adapted, introducing a Ge-precursor into the solution.

When Ge-precursor, Germanium Isopropoxide (IV) (GeIPO), was introduced with 1% of molar ratio GeIPO/ZnAc, the color of the solution changed immediately to white, and the final films must be transparent. To solve this problem, two different solutions were prepared: the first one, called A, involves the synthesis of ZnO with IPA, and the second one, called B, with a solution of 10% molar of GeIPO into IPA.

The solutions were deposited onto silicon substrates by spin coating at a speed of 2000 rpm for 30 seconds. This process was made layer-by-layer, one layer of A, followed by a pre-treatment at 300ºC for 1 or 10 minutes, one layer of B, and the same treatment. The annealing treatment was made at 500ºC for 1 hour at room conditions.

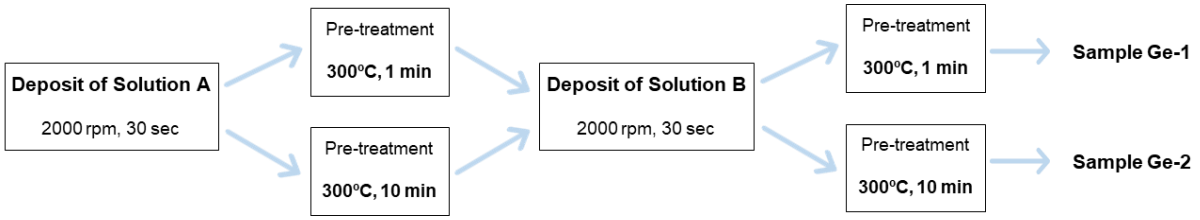

Figure 7 *– Schematic representation of Ge-1 and Ge-2 samples preparation using Ge- and Zn-precursors in different starting solutions.*

To understand the active role of water in the reaction, the influence of air moisture was studied. Indeed, the first attempts of synthesis were made in the spring months with very high humidity. In the summer period, first approach was repeated, increasing the concentration of dopant. So, two different syntheses routes were analyzed: in the first solution (Synthesis I), GeIPO was added in the beginning at the same time that ZnAc, while in the second solution (Synthesis II) was only added after 30 minutes.

For Synthesis I, 200 mg of ZnAc was dissolved in 0.9 mL of ethanol (EtOH). Then, 5.5 µL of GeIPO (2% of theoretical doping) and 0.066 mL of MEA were added under stirring at 60°C to provide a transparent solution. After 30 minutes, 0.35 mL of EtOH was added, and the solution was deposited on the substrate after more 5 minutes of stirring.

For Synthesis II, 200 mg of ZnAc was dissolved in 0.9 mL of EtOH. Then, 0.066 mL of MEA was added under stirring at 60ºC to provide a transparent solution. After 30 minutes, 5.5 µL of GeIPO was added, and an additional stirred was performed for more 30 minutes. Finally, 0.35 mL of EtOH was added, and the solution was deposited on the substrate after more 5 minutes of stirring.

Each solution originated three samples with one, two or three layers. The deposition was made onto silicon and fused silica substrates at 2000 rpm for 1 minute, followed by fast drying in a hot plate at 300°C for a few seconds. The samples were treated under a UV lamp to destroy the organic ligands for

2 minutes and finally treated again at 300°C for 5 minutes to complete the crystallization. The films must cool down before performing a further layer deposition. The thermal treatment was performed at 500°C at room atmosphere for 1 hour with a ramp of 10°C/min.

3.1.3. SiZO thin films

Si-doped ZnO thin films produced by Sol-Gel spin coating are already reported in the literature [67]. For this reason, the synthesis was reproduced to understand if it effectively works. So, 4 mmol of ZnAc was dissolved in 10 mL of 2-propanol (IPA) and stirring at 60°C for 10 minutes. During stirring, 4 mmol of DEA was added drop by drop, and then Tetraethylorthosilicate (TEOS) was added to give a 1.5% mole ratio of TEOS/ZnAc. Finally, the solution was stirred for more 10 minutes, during which time distilled water was added.

The first challenge is related to the amount of water that we should add to obtain a transparent and homogeneous solution. To overcome the problem, two solutions were prepared: one without water and another one adding it until seeing the flocculation phenomenon.

Each solution originated a sample with two layers. The deposition was made by spin coating at 2000 rpm for 30 seconds onto silicon substrates. Between each layer, the films were dried at 300ºC for 1 minute to remove organic ligands, and the final post-treatment ran at 500ºC for 1 hour with a ramp of 5ºC/min.

The role of the Silicon-dopant was also studied, reproducing again the synthesis developed for ZnO thin films with 1.5% molar ratio of Si-dopant/ZnAc and, in the final step, introducing the Silicon Tetrachloride ($SiCl_4$). The deposition and pre- and post-treatment were the same as the described above for TEOS.

To understand the role of thermal annealing, the first synthesis with 5% mole ratio of TEOS/ZnAc was repeated using fused silica substrate. The deposition was the same as described above. The post-treatment was performed in a hydrogen atmosphere, at 500ºC for 1 hour, and then at room atmosphere for 1 more hour at the same temperature.

Evaluated the amount of water, the different dopant precursors and the atmosphere environment, the final procedure was produced. So 0.44 g of ZnAc was dissolved in 5 mL of IPA and stirring for 10 minutes at 60ºC. During stirring, 0.21 g of DEA was added drop by drop. After this, TEOS was added to give one of three different Si/Zn molar ratios: 1.5%, 3%, and 6%. The solution was stirred for more 10 minutes and then was cooled down slowly.

Six different samples were prepared, using silicon and fused silica substrates, with two or three layers. Between each layer, the samples were dried at 300ºC for 1 minute and then subjected to UV treatment for 5 minutes, to guarantee the total elimination of organic ligands.

The post-treatment was performed at 500ºC for 1 hour at room atmosphere, to promote the formation of zinc oxide, and then was performed another treatment in hydrogen conditions, at 400ºC for 1 hour, to

increase the concentration of zinc vacancies.

3.2. Characterization and results

3.2.1. ZnO thin films

The crystal structure of ZnO thin films was characterized using XRD. Figure 8 shows the existence of predominant reflection planes, which proves that films have a polycrystalline nature. The obtained peaks correspond to the XRD patterns of the ZnO pattern from the JCPDS data (JCPDS Nº 36-1451), having a wurtzite hexagonal structure with lattice constants $a = 3{,}250$ Å and $c = 5{,}207$ Å [49].

The experimental structural parameters can be calculated using equations (12) and (13). The first one, the Bragg's Law, gives the interplanar spacing (d), while the second one allows to obtain the lattice constants (a and c).

$$d\,(\text{Å}) = \frac{\lambda}{2\sin\theta} \tag{12}$$

Where λ is the wavelength of the incident light and θ is the diffraction angle in radians.

$$\left(\frac{1}{d}\right)^2 = (h^2 + k^2 + h\cdot k)\cdot A + l\cdot C^2 \tag{13}$$

Where (h k l) is the Miller index and a and c are given for equations (14) and (15), respectively.

$$a\,(\text{Å}) = \frac{2}{A\cdot\sqrt{3}} \tag{14}$$

$$c\,(\text{Å}) = \frac{1}{C} \tag{15}$$

Table 1 shows the calculated values, that agree with JCPDS data. The precursor concentration was found to not affect these parameters.

***Table 1** – Calculated interplanar spacing and lattice constants for different Zn-precursor concentrations.*

Sample	Concentration	d $_{(002)}$ (Å)	d $_{(101)}$ (Å)	a (Å)	c (Å)
ZnO-1	As made	2,605	2,476	3,357	5,210
ZnO-2	½	2,598	2,479	3,368	5,195

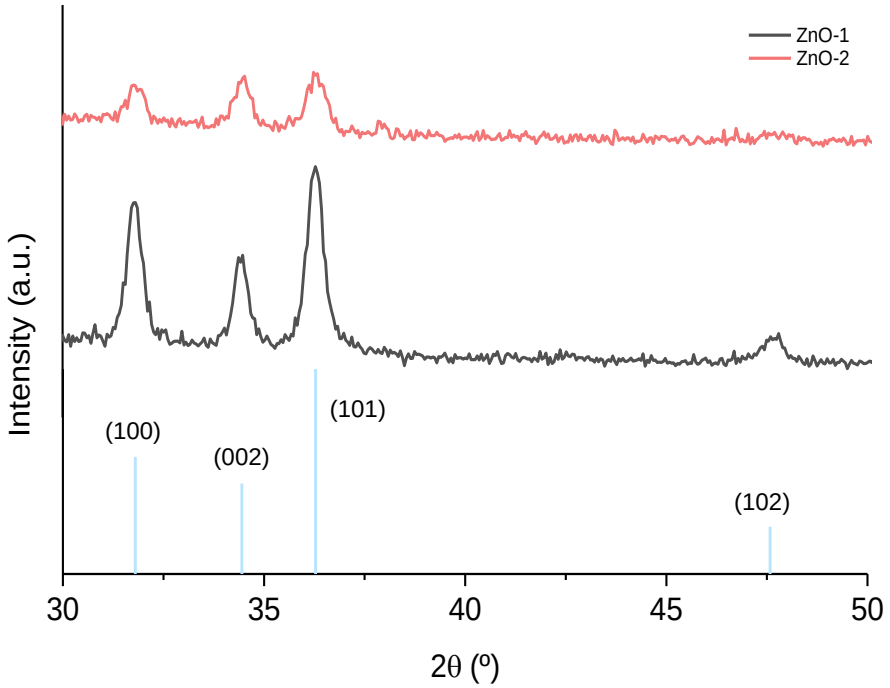

***Figure 8** – XRD patterns for ZnO thin films deposited by spin coating with different precursor concentrations and theoretical diffraction peak position for ZnO (JCPDS Nº 36-1451).*

The crystallite size was estimated using the Scherrer Equation (equation (16)).

$$D\ (nm) = K\ \frac{\lambda}{\cos\theta \cdot \Delta(2\theta)} \tag{16}$$

Where D is crystallite size, K is the shape factor with a value close to unit (it was used 0,9), λ is the wavelength of x-rays (in this case, 1,5406 Å), θ the diffraction angle in radians and $\Delta(2\theta)$ the Full Width at Half Maximum (FWHM) of the diffraction peak.

Table 2 shows the FWHM and the crystallite size along the prominent diffraction plane. The film thickness and refractive index (n) obtained by Spectroscopic Ellipsometry are also shown in Table 2.

Table 2 *– Structural parameters and refractive index (λ=600 nm) for ZnO thin films with different precursor concentrations.*

Sample	FWHM	Crystallite Size (nm)	Thickness (nm)	Refractive Index (n)
ZnO-1	0,47	17,6	103	1,68
ZnO-2	0,54	15,3	42	1,64

Analyzing the effect of concentration, a better crystallization is observed for the most concentrated film, which corresponds to an increase of the thickness. Moreover, for the sample with half concentration, crystallite size decreases slightly, but thickness has a reduction of 60%. Some studies reported an increase in carrier mobility and a decrease of sheet resistance for higher values of thickness, which provide superior electrical properties [68]. However, increasing the thickness, the transmittance may become poorer [3]. Weighted value of thickness must be chosen to have a balance between optical and electrical properties, without degrading both considerably.

The refractive index is higher for the higher value of film thickness and, consequently, for the most concentrated sample. However, this parameter is lower compared to the theoretical value for ZnO, $n = 2$, at λ= 600 nm [69].

XRD patterns (Figure 8) also revealed a decrease in the preferential crystal growth orientation along (101) plane when the precursor concentration decreases. It is already reported that the sol concentration affects the preferential orientation growth [47,70].

During the first layer pre-treatment, the formed nuclei grow slowly into crystal, preferentially along the (002) plane (c-axis), because this plane has a minimum surface free energy and, consequently, has the most kinetically favored growth. After that, when the second layer is coated and pre-heated, the first one acts as a template, and the newly formed crystal can grow into other directions more than c-axis orientation. It explains the different main orientation along (101) plane.

The temperature of pre-treatment also influences the preferential growth, because it must be higher than 200ºC to guarantee the total vaporization of solvents and organic compounds. However, the thermal decomposition temperature of Zinc Acetate is 240ºC, while the crystallization of ZnO begins between 200-300ºC. Since a pre-treatment at 300ºC was used, the two phenomena may occur almost simultaneously, changing the structural relaxation time, and, consequently, films have a random distribute configuration [71].

Figure 9 shows the surface morphology of the ZnO-1 thin film. The film is uniform, presenting a small grain size, which was already revealed by XRD and confirmed by the calculated crystallite size (Table 2).

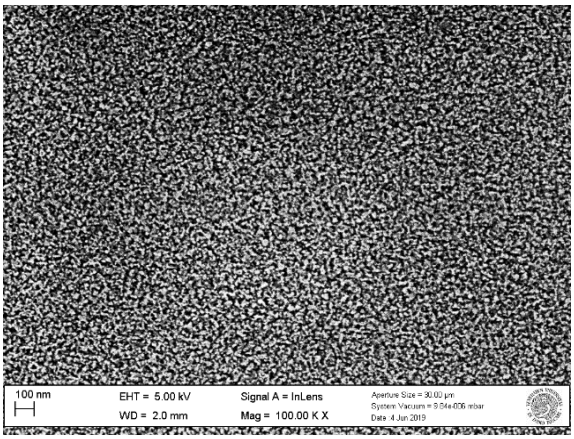

Figure 9 *– SEM micrograph of ZnO-1 thin film.*

The use of different chelating agents does not influence the lattice parameters (Table 3). Employing DEA as a chelating agent, the films also show a crystalline structure for the prominent diffraction plane (Table 4). Comparing with the MEA results (Table 2), they have similar values for crystallite size and the same effect of concentration. The films demonstrate (101) preferential orientation, independently of the precursor concentration (Figure 10). It suggests that DEA and MEA have the same behavior. However, other studies concluded that the OH groups of DEA form stronger bonds with Zn^{2+}, causing a higher nucleation barrier. For this reason, DEA can act as an inhibitor of the crystallization in the (002) direction, the more kinetically favored plane of growth [72].

Table 3 *– Calculated interplanar spacing and lattice constants of ZnO thin films prepared with DEA as a chelating agent and different Zn-precursor concentrations.*

Sample	Concentration	d $_{(002)}$ (Å)	d $_{(101)}$ (Å)	a (Å)	c (Å)
ZnO-3	As made	2,601	2,473	3,350	5,203
ZnO-4	½	2,609	2,473	3,347	5,217

Table 4 *–Structural Parameters for ZnO thin films prepared with DEA as a chelating agent and different Zn-precursor concentrations.*

Sample	Concentration	FWHM	Crystallite Size (nm)
ZnO-3	As made	0,45	18,6
ZnO-4	½	0,52	15,9

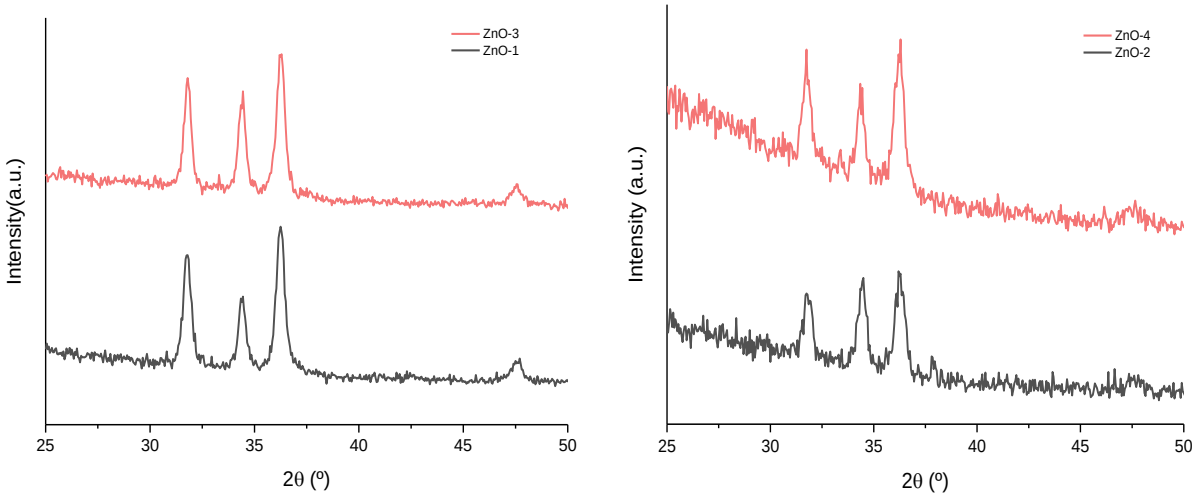

Figure 10 *– Comparison of XRD patterns for ZnO thin films using different stabilizer agents (MEA in black and DEA in red) and different Zn-precursor concentrations.*

The study of different reaction times by XRD is shown in Figure 11. All the films have a good crystallization, independently of the reaction time. The crystallite size only changes and becomes higher when a reaction takes time for 7 hours. However, for this time, the thickness and the refractive index are almost the same for 30 minutes. It means that it could be necessary to wait a long time, such as several days, to obtain a considerable difference in structural parameters. Therefore, does not make sense to wait a long time to get the same results.

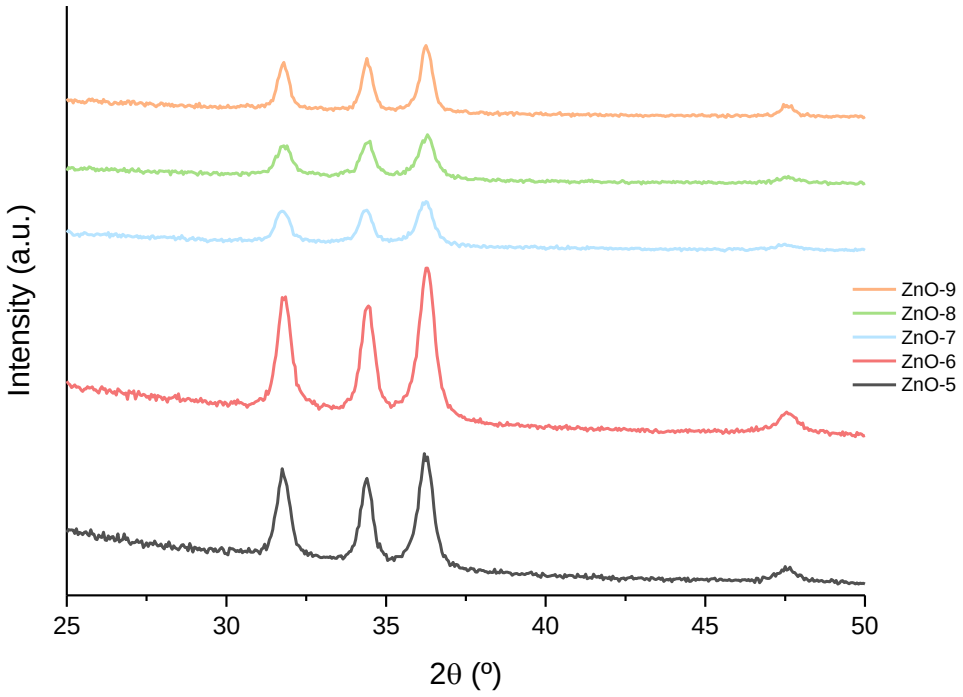

Figure 11 *–XRD patterns for ZnO thin films with different reaction times using MEA as a chelating agent and the higher studied Zn-precursor concentration.*

***Table 5** – Structural Parameters and refractive index (λ=600 nm) for ZnO thin films with different reaction times using MEA as a chelating agent and the higher studied Zn-precursor concentration.*

Sample	Reaction Time (h)	FWHM	Crystallite Size (nm)	Thickness (nm)	Refractive Index
ZnO-5	0,5	0,50	16,6	109	1,62
ZnO-6	1	0,56	15,1	115	1,59
ZnO-7	2	0,56	14,9	122	1,56
ZnO-8	4	0,49	16,9	126	1,58
ZnO-9	7	0,40	20,7	107	1,65

A FTIR spectrum of ZnO-5 (Figure 12) shows the Zn-O stretching vibrations at 435 and 449 cm^{-1} that guarantee a complete transformation of $Zn(OH)_2$ into ZnO. The absence of C=O correspondent peak around 1385 cm^{-1} and O-H deformation vibration near 1600 cm^{-1} demonstrates the total evaporation of acetate groups and non-existence of intermediate species formed in the hydrolysis of Zinc Monoacetate, respectively [63,73].

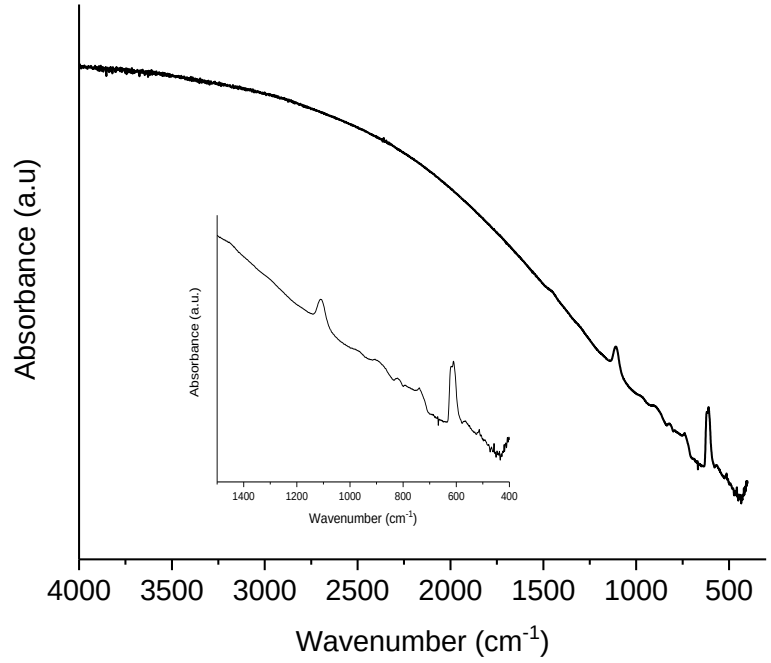

***Figure 12** – FTIR spectrum of ZnO-5 sample showing Zn–O bonding at 435 and 449 cm^{-1}.*

The role of some specific parameters of the ZnO thin film synthesis were studied to allow to develop a final one that can be used as a starting point for the synthesis of ZnO-doped films. Due to the higher number of variables involved in the sol-gel approach, all temperatures and all deposition parameters were set, because it is easy to find a good agreement with them in literature.

Analyzing the results, the higher studied concentration provides a better crystallization and a pondered thickness is necessary to obtain good electrical and optical properties for ZnO-doped films. Using MEA, the higher nucleation barrier is avoided which provides well orientated films and applying a short reaction time is enough to guarantee the formation of ZnO.

3.2.2. GeZO thin films

Preparing a solution with both water and germanium alkoxide together, the instantaneous formation of a turbid solution was observed, ascribable to the fast hydrolysis and condensation reactions of germanium precursor. Indeed, the presence of water catalyzes the reactions very fast and leads to the formation of Ge–O–Ge homocondensation products [74].

One of the most common applied methods to retard hydrolysis and condensation processes in the presence of water is the use of stabilizing agents [75]. Acetylacetone is a well-known type of agent for different metal alkoxides. It behaves as a chelating rather than as a bridging ligand and it decreases the high reactivity of them. However, for germanium alkoxides, even in the presence of Acetylacetone, reactions occur immediately, developing a milky solution [74]. Unfortunately, any known stabilizers are effectively able to retard these reactions for Ge-alkoxides precursors.

Figure 13 shows the XRD measurements of Ge-1 and Ge-2 samples, obtained from two separated starting solutions. Both thin films are polycrystalline with three main peaks, indicating the formation of ZnO nanocrystals (JCPDS Nº 36-1451). It is possible to observe a changing in preferred growth, which is (002) plane for samples with germanium.

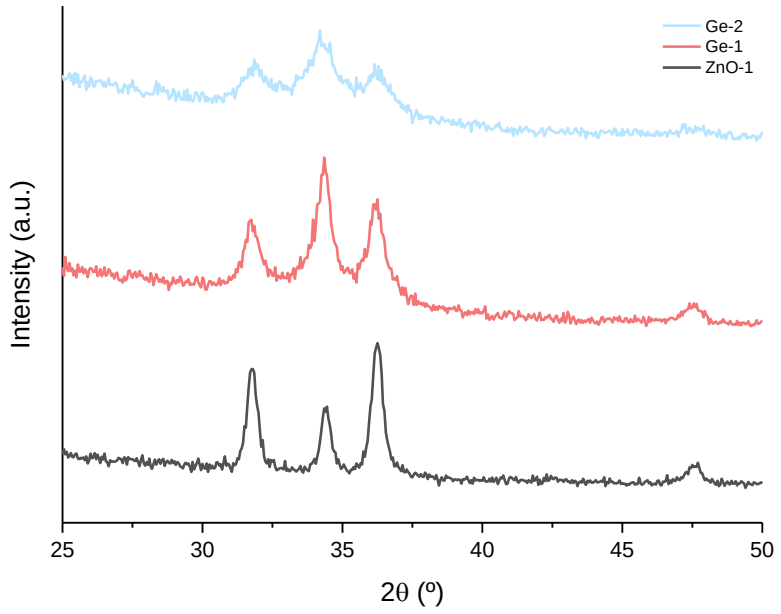

Figure 13 *– XRD patterns of GeZO thin films prepared from two different starting solutions with different pre-treatment time (1 minute (in red) and 10 minutes (in blue)) and of undoped ZnO thin film.*

The lattice parameters presented in Table 6 were estimated by equations (12)-(15). For sample Ge-2 there is an increase in all parameters. If Ge ions are incorporated in the ZnO structure, atoms will rearrange due to the placed Ge as an interstitial ion [24]. However, Ge ions have a lower radius than Zn ions, and, consequently, the lattice parameters must decrease. Moreover, the analysis of XRD patterns in Match! Program revealed the presence of Zn_2GeO_4 (JCPDS Nº 25-1020 and Nº 25-1018), which can be responsible for higher values. For these reasons, real doping cannot be expected.

Table 6 *– Calculated interplanar spacing and lattice constants of different GeZO thin films prepared from two separated starting solutions and of ZnO-1 thin film.*

Sample	Pre-heating time (min)	d $_{(002)}$ (Å)	d $_{(101)}$ (Å)	a (Å)	c (Å)
ZnO-1	1	2,605	2,476	3,357	5,210
Ge-1	1	2,609	2,476	3,356	5,217
GE-2	10	2,620	2,483	3,369	5,239

Another interesting fact is the decreases of crystallite size with the increasing of pre-heating time (Table 7). Some studies reported a considerable influence of pre-treatment temperature in the crystal growth of ZnO thin films. Increasing the temperature, the vaporization of the solvent and the decomposition of ZnAc can occur abruptly and simultaneously with crystallization, decreasing the crystallite size [76]. The results show that probably the use of a pre-heating time of 1 minute is not enough to allow that all the samples reach a homogenous temperature of 300ºC, which might explain the difference in crystal size, when compared to the pre-heating time of 10 minutes.

Table 7 *– Structural Parameters for different GeZO thin films prepared from two separated starting solutions.*

Sample	Pre-treatment time (min)	FWHM	Crystallite Size (nm)
Ge-1	1	0,56	14,9
Ge-2	10	1,00	8,3

Figure 14 shows the surface morphology of the Ge-1 sample. The result is almost the same as XRD, with grain size small and uniform. There are some pores on the surface, which are related to the decomposition reaction of the precursor and the evaporation of residual organics in gel films [77].

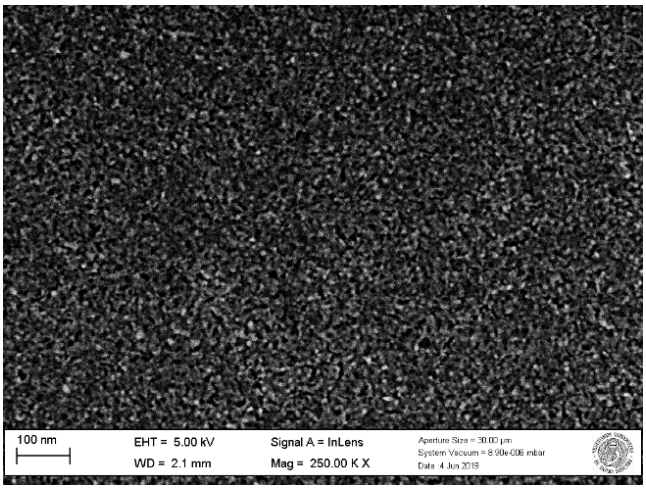

Figure 14 *– SEM micrograph of Ge-1 thin film.*

In summer months, when air moisture was lower than the spring period, it was possible to repeat the first approach and to obtain a transparent solution. It shows the huge impact of water and relative humidity in reaction. Some articles report the use of inert atmosphere glove box, with water and oxygen levels controlled, to prevent simple hydrolysis of the Ge-precursor [22].

Figure 15 shows the XRD patterns of samples obtained from Synthesis I, with a different number of layers. All of them exhibit the three main peaks, correspondent to those of ZnO patterns from the JCPDS data. The films were polycrystalline and randomly orientated. However, it is not possible to achieve narrow and well-defined peaks due to the deterioration of the ZnO crystallinity with the introduction of defects [37].

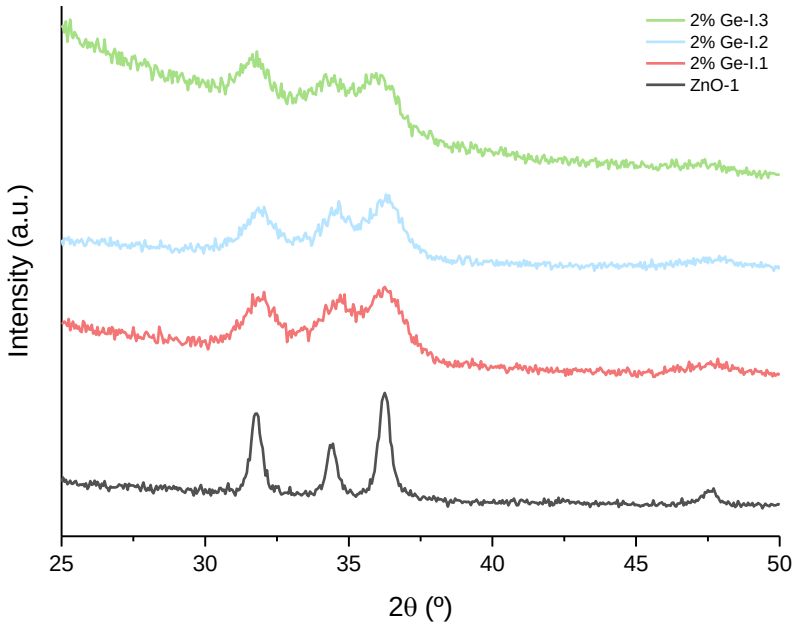

Figure 15 *– XRD patterns for GeZO thin films prepared from Synthesis I with different number of layers.*

Table 8 shows the lattice parameters for samples obtained from Synthesis I. Analyzing them, it is not possible to predict a tendency increasing the number of layers. However, for 2% Ge-I.2 thin film, both values a and c decrease, which could represent the introduction of impurities in the lattice site.

***Table 8** – Calculated interplanar spacing and lattice constants of different GeZO films prepared from Synthesis I and of ZnO-1 thin film.*

Sample	Number of layers	d $_{(002)}$ (Å)	d $_{(101)}$ (Å)	a (Å)	c (Å)
ZnO-1	2	2,605	2,476	3,357	5,210
2% Ge-I.1	1	2,572	2,477	3,371	5,144
2% Ge-I.2	2	2,587	2,473	3,355	5,173
2% Ge-I.3	3	2,620	2,496	3,403	5,239

As previously revealed by XRD patterns, the crystallite size decreases abruptly with the introduction of Ge-dopant (Table 9). As expected, the thickness increases with the increases in the number of layers.

***Table 9** – Structural Parameters of different GeZO films prepared from Synthesis I and ZnO-1 thin film.*

Sample	Number of layers	FWHM	Crystallite Size (nm)	Thickness (nm)
ZnO-1	2	0,47	17,6	103
2% Ge-I.1	1	1,38	6,1	77
2% Ge-I.2	2	1,17	7,1	126
2% Ge-I.3	3	1,70	4,9	160

For films prepared from Synthesis II, the presence of Ge ion as a dopant contributes to the distortion in lattice parameters, with a decrease in crystallite size as a consequence. However, analyzing Figure 16, the film with 3 layers shows the three main peaks with higher intensity compared with the same sample prepared from Synthesis I (Figure 15).

Observing Table 10, the lattice parameters change in the same way that was reported for samples from synthesis I (Table 8). Again, the film with two layers is the only that shows a decrease in both a and c parameters.

The crystallite size decreases when the number of layers increases (Table 11). The incorporation of Ge reduces the proportion of Zn in the film, which reduces the diffusivity of ZnO and suppresses the growth of grain in the film [37]. To note that a decrease in crystallite size can help to improve the photocatalytic activity.

For synthesis II, all the films exhibit a lower thickness comparing with the correspondent sample obtained from Synthesis I (Table 9). However, the difference is not significant.

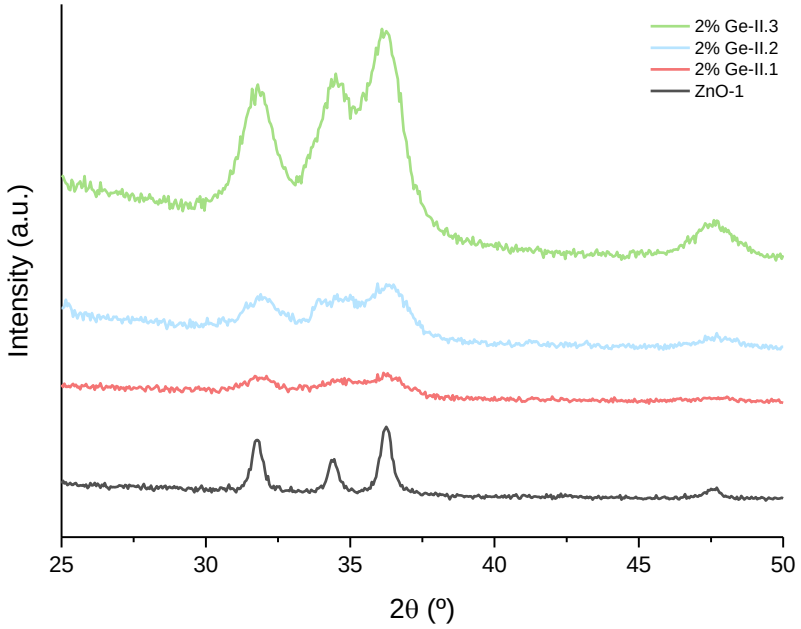

Figure 16 *– XRD patterns for GeZO thin films prepared from Synthesis II with different number of layers.*

Table 10 *– Calculated interplanar spacing and lattice constants of different GeZO films prepared from Synthesis II and ZnO-1 thin film.*

Sample	Number of layers	d $_{(002)}$ (Å)	d $_{(101)}$ (Å)	a (Å)	c (Å)
ZnO-1	2	2,605	2,476	3,357	5,210
2% Ge-II.1	1	2,576	2,483	3,385	5,152
2% Ge-II.2	2	2,594	2,460	3,319	5,188
2% Ge-II.3	3	2,620	2,486	3,386	5,195

Table 11 *– Structural Parameters of different GeZO films prepared from Synthesis II and ZnO-1 thin film.*

Sample	Number of layers	FWHM	Crystallite Size (nm)	Thickness (nm)
ZnO-1	2	0,47	17,6	103
2% Ge-II.1	1	1,22	6,8	70
2% Ge-II.2	2	1,35	6,2	112
2% Ge-II.3	3	1,72	4,9	163

Figure 17 shows the surface morphology of the 2% Ge-II.3 sample. The film is uniform with a small grain size, which was already demonstrated by XRD pattern (Figure 16).

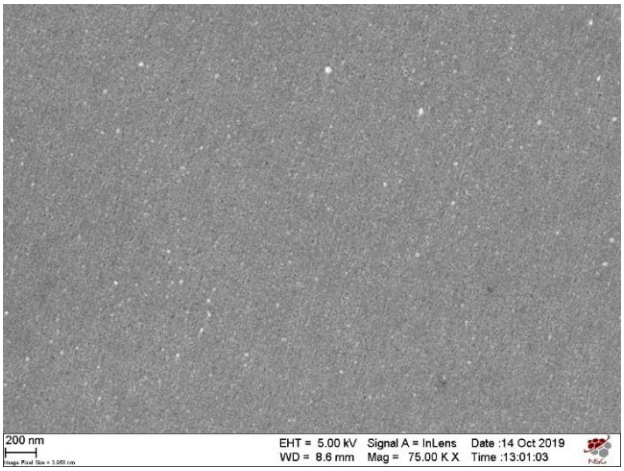

Figure 17 *– SEM micrograph of 2% Ge-II.3 thin film.*

The EDS analysis of the film (Figure 18) reveals the presence of Germanium in the GeZO, but the real doping appears to be higher respect to the nominal ratio – around 5-6% instead of 2% (Appendix B). This result is due to, probably, a not good calibration of the instrument's sensor. However, it is possible to consider it as a qualitative analysis. The EDS result also shows the presence of Zinc, Oxygen, Germanium and Silicon. The Silicon is from the substrate.

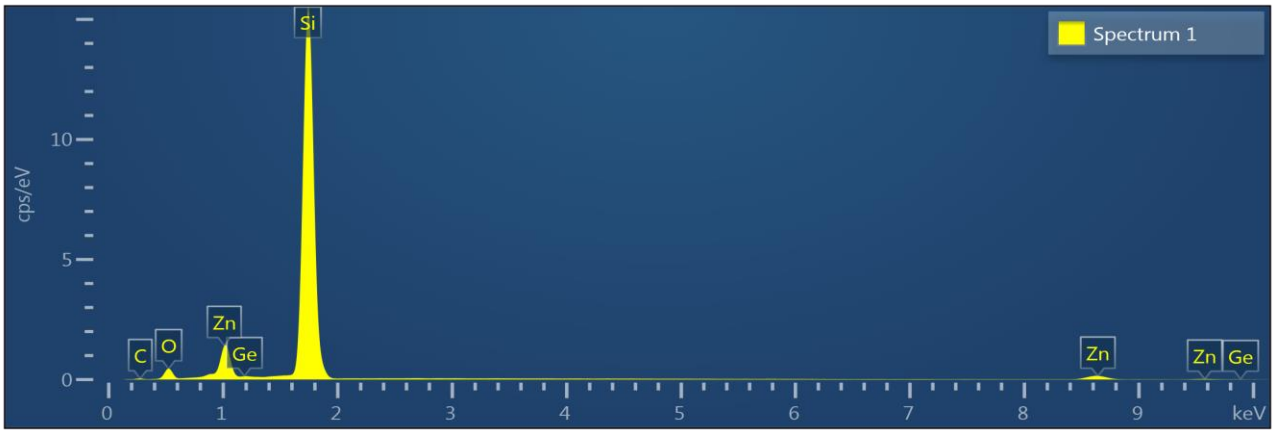

Figure 18 *– EDS analysis of 2% Ge-II.3 thin film.*

Comparing the results obtained from films prepared from both different syntheses, it is possible to conclude that they have the same behavior with the same results.

From the Spectrometric Ellipsometry (Appendix A.2), the variation of refractive index (n) and extinction coefficient (k) were measured. The absorption coefficient (α) and k are related by equation (17) [49].

$$\alpha\ (nm^{-1}) = \frac{4\pi \cdot k}{\lambda} \qquad (17)$$

Figure 19 represents the refractive index for different synthesized films. First of all, it is clear that n decreases with the increase of the wavelength. Films with the same number of layers have a similar n for different wavelengths, although samples prepared from Synthesis I exhibit higher values. It is possible to observe an increase of n when the number of layers and the thickness increase.

For a wavelength of λ= 600 nm, ZnO has n= 2. The lower values obtained for GeZO samples can be attributed to several factors: on the one hand, it is due to the decreased polarizability of the smaller Ge atomic radius compared with Zn atomic radius, and on the other hand, it is due to looser surface or the presence of GeO_2 [78]. However, the XRD patterns do not evidence the existence of this oxide.

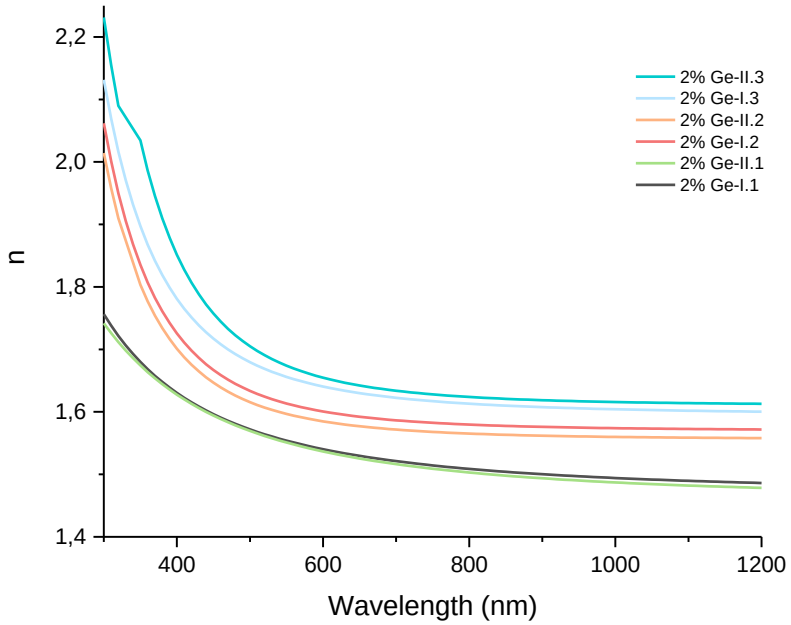

Figure 19 *– Refractive index of GeZO thin films prepared from both Synthesis I and II.*

The absorption coefficient trends for different GeZO thin films are shown in Figure 20. In the wavelength range of 400-700 nm, correspondent to the visible part of the spectrum, α is very low, which means that all films studied in this work are homogeneous and highly transparent.

In UV region, similar values for samples with the same number of layers were observed. However, unlike it happens with n, the higher values of α correspond to the samples with 2 layers. The increase in the thickness can be excessive, decreasing α.

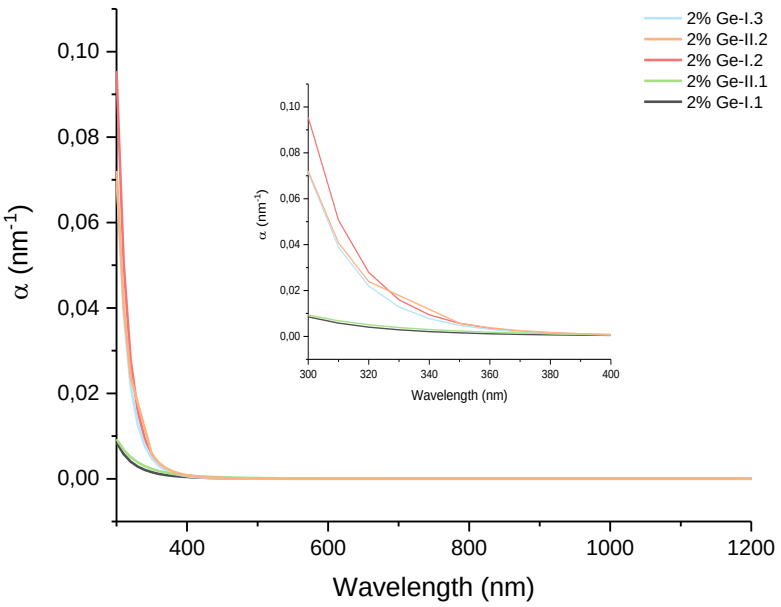

Figure 20 *– Absorption coefficient of GeZO thin films prepared from Synthesis I and II.*

In order to measure the optical properties, Solution I and Solution II were deposited onto fused silica substrates with 3 layers. In Figure 21, it is possible to observe the different crystal growth using different substrates. Usually, amorphous substrates, like fused silica, lead to oriented films along the (002) direction because they are non-bridging oxygen atoms. On the other hand, using well-crystallized silicon substrates, whose a parameter is very close to the c parameter of the hexagonal cell of ZnO, helps to obtain the desired crystallization [51].

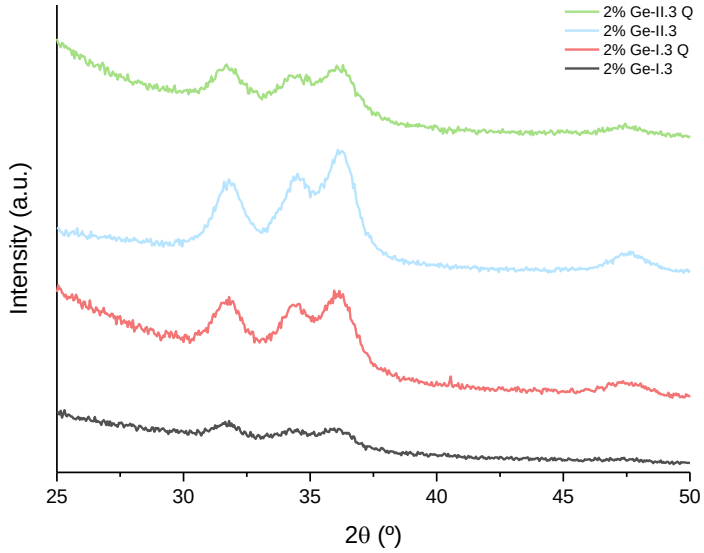

Figure 21 *- XRD patterns of GeZO thin films prepared from Synthesis I and II with 3 layers onto fused silica substrate.*

Table 12 present the lattice and structural parameters for GeZO thin films obtained from Synthesis I and Synthesis II and deposited onto fused silica substrate. Although the XRD patterns are different for

distinct substrates, the lattice parameters always have the same evolution. The crystallite size has similar values, independently of the substrate.

The films deposited onto silicon and fused silica substrates were prepared at the same time. For this reason, the same thickness was considered for both substrates.

***Table 12** – Calculated interplanar spacing and lattice constants, and structural parameters of GeZO films prepared from Synthesis I and Synthesis II with 3 layers and deposited onto fused silica substrate.*

Sample	d $_{(002)}$ (Å)	d $_{(101)}$ (Å)	a (Å)	c (Å)	FWHM	Crystallite Size (nm)
ZnO-1	2,605	2,476	3,357	5,210	0,47	17,6
2% Ge-I.3 Q	2,595	2,496	3,413	5,189	1,84	4,5
2% Ge-II.3 Q	2,619	2,472	3,344	5,238	1,68	4,9

Figure 22 shows the absorption spectra of GeZO with 3 layers deposited onto fused silica substrate. The films exhibit low absorbance in the visible region, which indicates transparency higher than 90%.

The spectra also show interference fringes, which are attributed to the interference of light reflected between air-film and film-substrate interface [28,49].

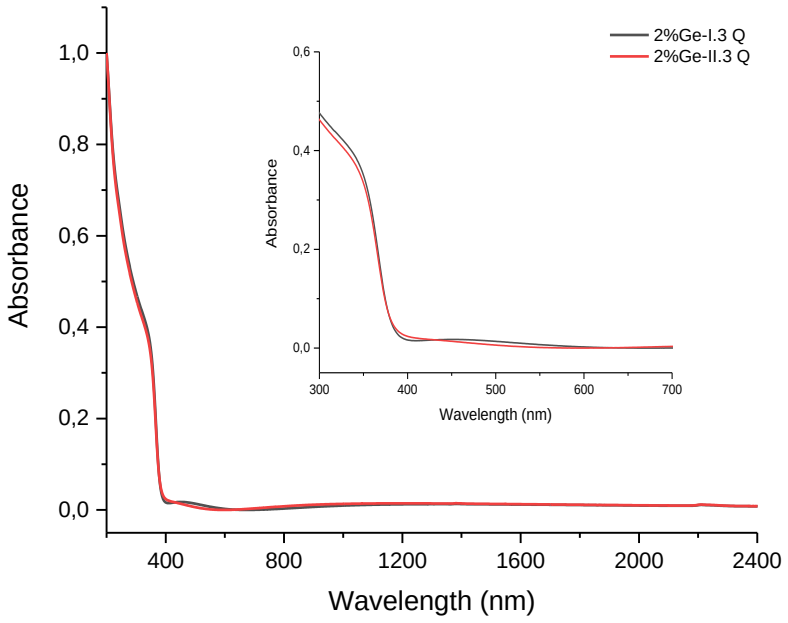

***Figure 22** – Absorption spectra of GeZO thin films prepared from Synthesis I (in black) and II (in red) with 3 layers deposited onto fused silica substrate.*

The Sheet Resistance of the films was measured using the Four-Probe Method (Appendix A.3). However, it was not possible to obtain stable results due to surface non-homogeneity of the samples and to the possible adsorption of humidity at the surface. For this reason, any data about electrical properties are reported.

3.2.3. SiZO thin films

In the first step, the amount of distilled water presented in the synthesis was evaluated. The XRD patterns for the films prepared with and without the addition of more water are shown in Figure 23. A well crystalize peaks were observed in both syntheses, although with the presence of some organic compounds, evidenced mainly for a peak around 2θ=42,7º.

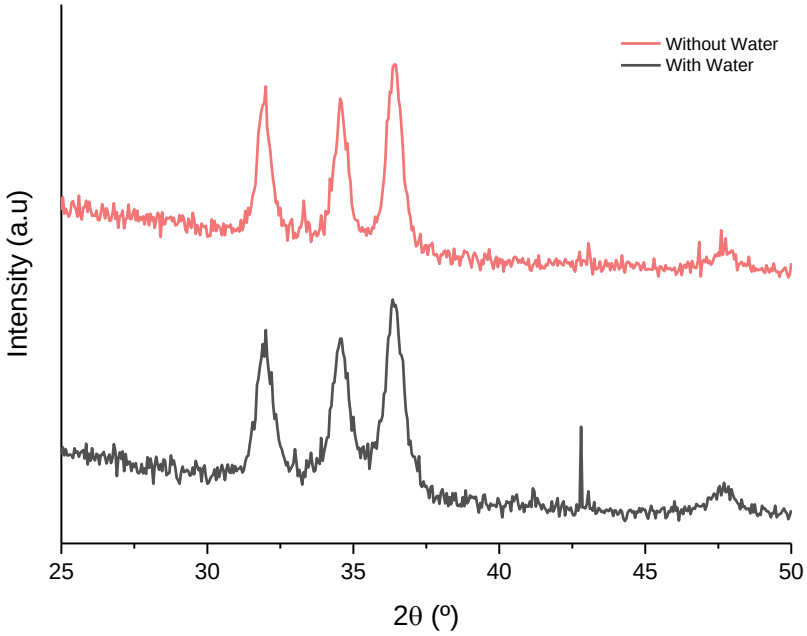

Figure 23 *– XRD patterns for SiZO thin films prepared using a synthesis with addition of water (in black) and a synthesis without addition of more water (in red).*

However, SEM pictures show a dendritic structure for the sample prepared with water, which indicates the existence of cracking in the film (Figure 24). Gel films develop tensile stress during heating, which is affected by several parameters, including the Water/Si-Alkoxide ratio. Indeed, for films prepared with higher ratios, the stress increases due to the higher capillary pressure. The capillary pressure is proportional to the surface tension of the vaporizing liquid, and the water surface tension is higher than that solvent, introducing the cracking [79]. Therefore, SiZO thin films must be synthesized without water.

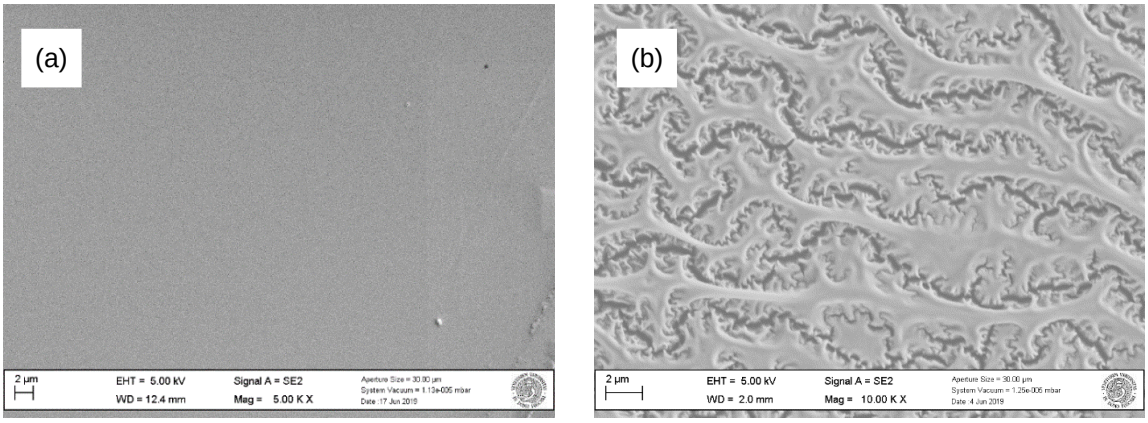

Figure 24 *– SEM pictures of SiZO thin films. (a) – Thin film obtained by synthesis without more addition of more water; (b) – Thin film obtained by synthesis with addition of water.*

Comparing the XRD results obtained for different Si-precursors, it is very clear the less crystallization of the sample with $SiCl_4$ as a precursor, contrasting with the TEOS sample (Figure 25). Moreover, $SiCl_4$ reacts immediately with water forming hydrochloric acid, making its handling dangerous. For these reasons, to synthesize films with TEOS and without the addition of more distilled water is the best approach to follow.

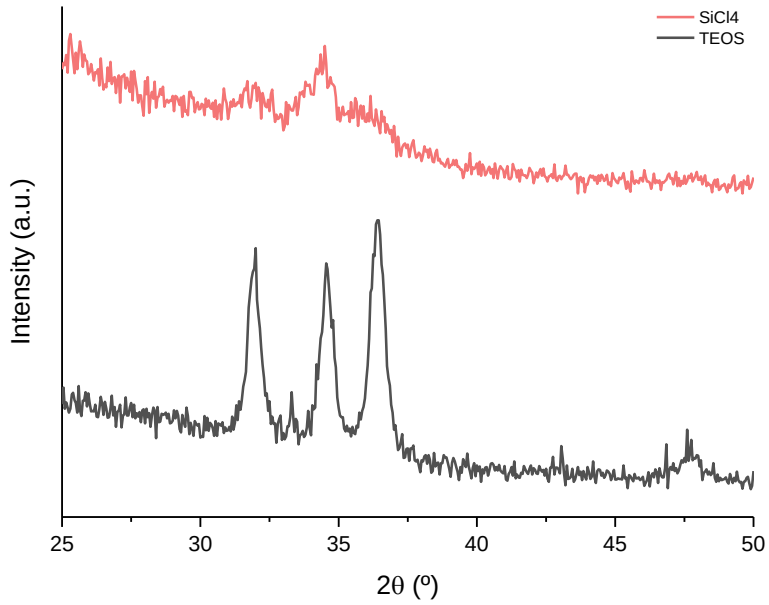

Figure 25 *– XRD patterns obtained of SiZO thin films prepared using different types of dopant precursors.*

From the study made with GeZO thin films, it is known the huge influence of substrate in the film crystallization. For this reason, the effect of thermal annealing atmosphere in fused silica substrate was studied because, indeed, several types can be used, such as air, vacuum, nitrogen, and hydrogen. However, the hydrogen atmosphere has as an advantage that H_2 easily diffuses into the solid structure,

even at low temperatures [80]. This treatment passivates the charge state of the zinc vacancies, improving the structural and electrical properties of the films [7].

Nevertheless, the obtained results were not expected because the samples present a brownish color (Figure 26), and it is not possible to observe any crystallization of ZnO using XRD measurement. The color can be due to the presence of organic compounds, so samples were annealed again in the presence of oxygen in room atmosphere to degrade them. However, although samples were transparent, it was not possible to detect any occurrence of ZnO crystallization.

Figure 26 *– Samples obtained after heat treatment in hydrogen conditions (on left) and the transparent color obtained after room atmosphere treatment.*

Figure 27 shows the XRD patterns obtained for films deposited onto a silicon substrate with 2 and 3 layers and different Si concentrations. With Si doping, the preferred orientation changes from (101) to (002) plane. The significantly increasing intensity of this peak proves the incorporation of defects ion in the lattice site. Moreover, the intensity of all peaks on the XRD decreases with the increase of doping concentration. It suggests the deterioration of the crystallinity of ZnO films due to the stress induced by the difference between ionic radii and the segregation of Si in the grain boundaries [37].

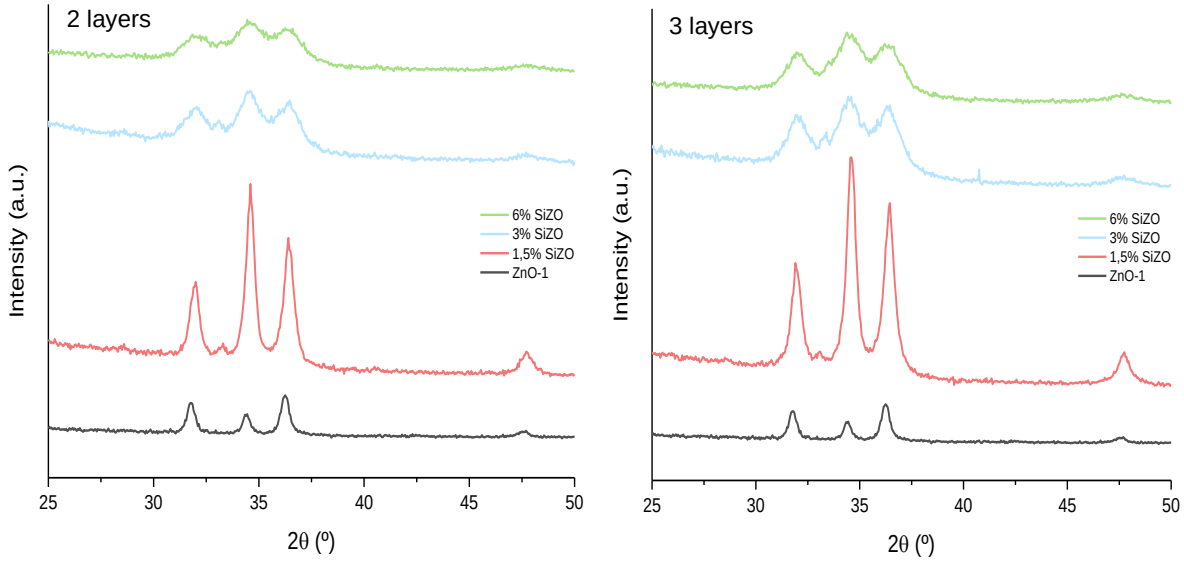

Figure 27 *– XRD patterns of SiZO thin films deposited onto silicon substrate with Si= 1.5%, 3% and 6% mol nominal. On the left, 2 layers; on the right 3 layers.*

Table 13 shows the calculated lattice parameters of films with different number of layers and different %Si content. With the introduction of the dopant, the lattice parameters of SiZO films are smaller than that of undoped ZnO. As Ge ions, Si ions have lower radius comparing with Zn ions, decreasing these parameters. There is no difference between the number of layers for the same Si concentration in the lattice parameters.

Table 13 *– Calculated interplanar spacing and lattice parameters of SiZO thin films prepared with different %Si content and different number of layers, and of ZnO-1 thin film.*

Sample	Number of layers	d $_{(002)}$ (Å)	d $_{(101)}$ (Å)	a (Å)	c (Å)
ZnO-1	2	2,605	2,476	3,357	5,210
1.5% SiZO	2	2,590	2,466	3,337	5,181
	3	2,593	2,463	3,328	5,185
3% SiZO	2	2,601	2,463	3,325	5,203
	3	2,601	2,463	3,325	5,203
6% SiZO	2	2,601	2,520	3,473	5,203
	3	2,605	2,479	3,366	5,210

The broadening peaks indicate a reduction in particle size of the SiZO films compared to that of ZnO. Indeed, this fact is verified with the calculated values, shown in Table 14. When silicon enters in ZnO structure as a dopant may tend to create more nucleation centers during the deposition process and, consequently, as a result of the increase of Si content, the crystallite size decreases [81]. The achieved thickness is similar for the same number of layers, independently the concentration of Si.

Table 14 *– Structural parameters obtained of SiZO thin films with different number of layers and different %Si content and of ZnO-1 thin film.*

Sample	Number of layers	FWHM	Crystallite Size (nm)	Thickness (nm)
ZnO-1	2	0,47	17,6	103
1.5% SiZO	2	0,45	18,6	154
	3	0,51	16,5	228
3% SiZO	2	1,38	6,0	152
	3	1,60	5,2	259
6% SiZO	2	1,58	5,3	164
	3	1,46	5,7	252

Figure 28 shows the surface morphology of 3% SiZO with 2 layers sample. The film surface is granular in nature with small grain size, already achieved by XRD measurement. It also possible to see some black areas due to the presence of organic ligands.

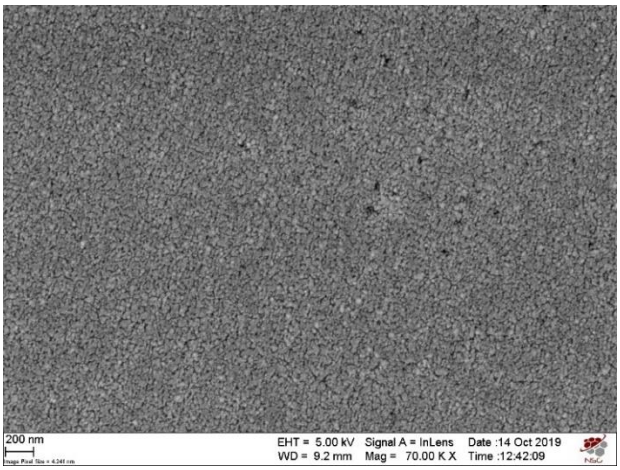

***Figure 28** – SEM micrograph of 3% SiZO with 2 layers thin film.*

Figure 29 shows the FTIR measurement for sample 1.5% SiZO with 2 layers. The formation of ZnO is verified for Zn-O stretching vibrations at 422 and 458 cm^{-1}. The concentration of dopant is very low, so it is not possible to see its correspondent vibrations. The vibration around 900 cm^{-1} is probably due to the contamination with SiO_2 from the substrate [63]. During the analysis, some moisture can be adsorbed, giving OH interferences – due to bending vibration of the OH bonds at 1640 cm^{-1} and due to stretching vibration of the OH groups at 3450 cm^{-1} [63]. On the other hand, the absence of other important bands proves the efficiency of the UV lamp in the total elimination of organic compounds during the deposition process. FTIR results for the other SiZO samples are not shown because they have the same behavior.

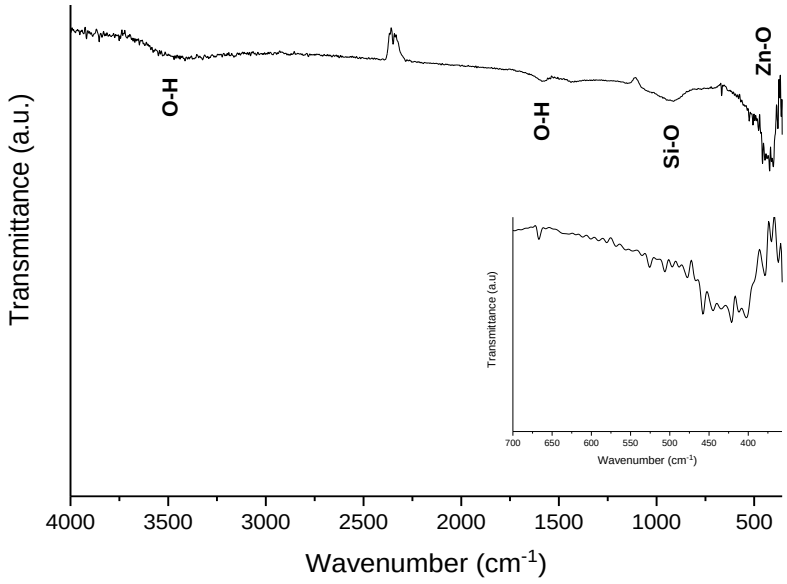

***Figure 29** – FTIR spectra of 1,5% SiZO sample with 3 layers deposited onto silicon substrate.*

From the Spectrometric Ellipsometry (Appendix A.2), the variation of refractive index (n) and extinction coefficient (k) were measured. The absorption coefficient (α) was calculated using equation 17.

Figure 30 and Figure 31 represent the refractive index and the absorption coefficient for different SiZO films. As observed in GeZO thin films, n decreases with the increase of the wavelength. Increasing the concentration of dopant, for the same wavelength, the value of n also increases. Differences in the number of layers do not affect n. For a wavelength of λ= 600 nm, ZnO has n= 2 and SiZO films always show lower values. This tendency was already reported and explained for GeZO films, in Chapter 3.2.2.

The absorption coefficient is very low in the visible region for all thin films, which means that they are homogeneous and highly transparent.

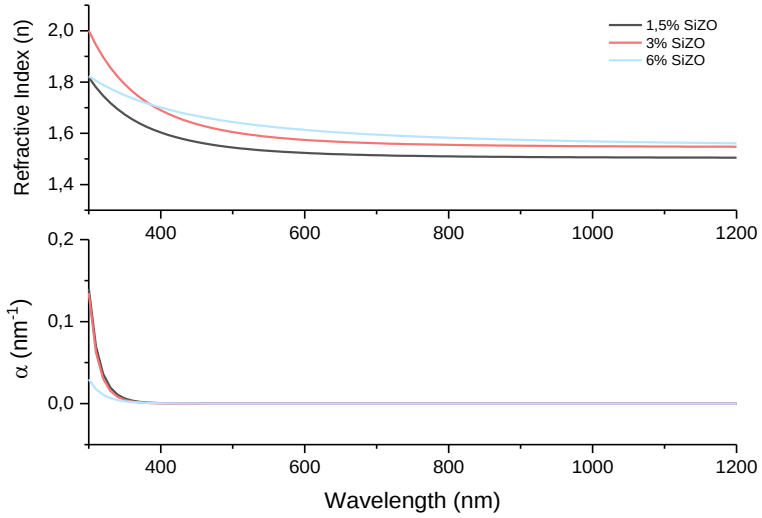

Figure 30 *– Refractive index n and absorption coefficient α of SiZO thin films with 2 layers and Si= 1.5%, 3% and 6% mol nominal.*

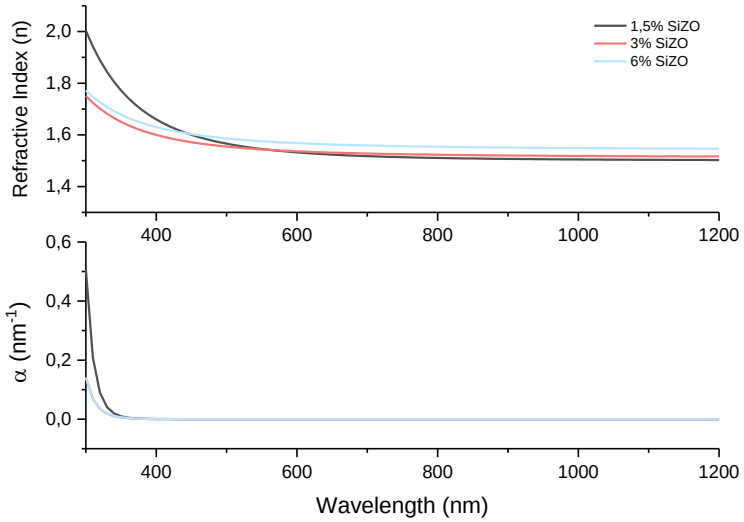

Figure 31 *– Refractive index n and Absorption Coefficient k of SiZO thin films with 3 layers and Si= 1.5%, 3% and 6% mol nominal*

To measure the optical properties, the same solutions were deposited onto fused silica substrate. Figure 32 shows the XRD patterns for these samples. It is clear that using fused silica substrates all SiZO films are amorphous. The dependence relationship with crystallization and nature of substrate was already achieved for GeZO and explained above in Chapter 3.2.2.

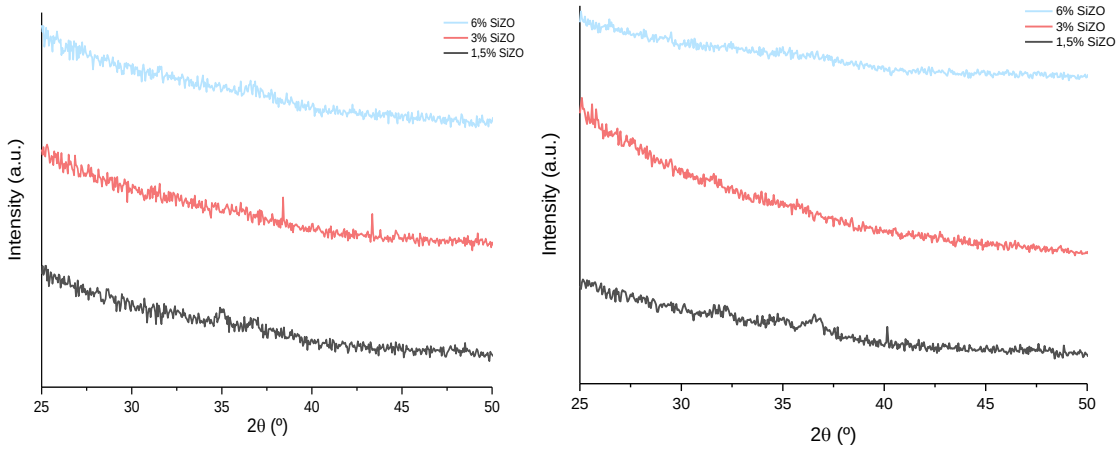

Figure 32 *– XRD patterns for SiZO thin films with 2 layers (left) and 3 layers (right) deposited onto fused silica substrate and Si= 1,5%, 3% and 6% mol nominal.*

Although the structure is amorphous, there is enough local ordering to see the optical absorbance [67].

Figure 33 and Figure 34 show the optical absorbance spectra for SiZO thin films with 2 and 3 layers, respectively. In the UV region, films exhibit high absorption, decay exponentially after the begging of the visible region (400 nm). The absorbance increases with increasing of Si doping concentration, and consequently, with the decrease in crystallite size, in both cases. This increase with Si doping may be due to the increase in morphological changes.

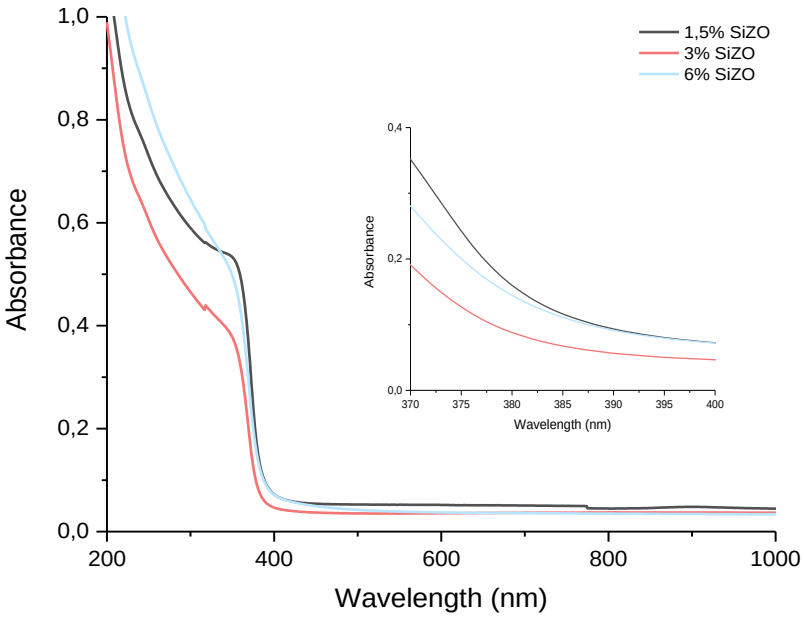

Figure 33 *– Optical Absorption spectra of SiZO thin films with 2 layers.*

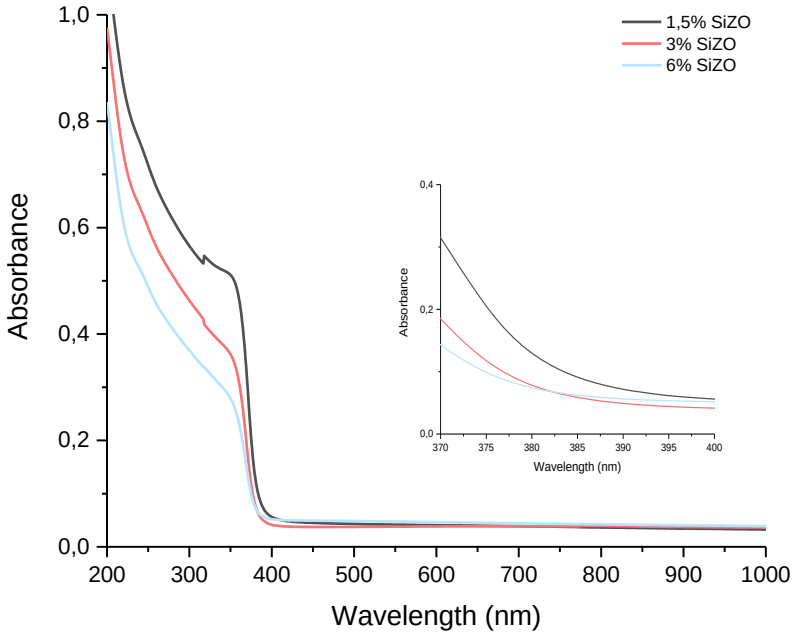

Figure 34 *– Optical Absorption spectra of SiZO thin films with 3 layers.*

As happen with GeZO was not possible achieve coherent values of the electrical properties. This problem was already justified in Chapter 3.2.2.

4. TCO thin films for photocatalytic applications

The photocatalytic activity of GeZO and SiZO thin films was evaluated by measuring the degradation of 2,6-dichloroindophenol under UV irradiation. Phenolic compounds and their derivates, like chlorophenols, are one of the most environmental pollutants, very toxics and hardly biodegradable. They are mainly discharged from textile and petrochemical industries, and petroleum refineries [39, 82].

Titanium dioxide (TiO_2) in anatase crystalline phase (JCPDS Nº 84-1285) was defined as a benchmark. It is a well-known photocatalyst generally used due to its low cost, non-toxicity, and chemical stability under UV radiation. Moreover, TiO_2 shows a Band Gap higher than 3,2 eV [41].

The ink solution was prepared with 45 mL hydroxyethyl-cellulose in 3 mL of water, 0.3 g of glycerol and 5 mg 2,6-dichloroindophenol which has a blue color. It was sonicated for 5 minutes and then stirred for more 30 minutes. The ink was deposited by drop cast onto the TCO layer, while the substrate was heated at 80ºC using a hotplate. After that, the samples were exposed to UV radiation in the dark.

The absorption spectrum of the ink was monitored by the UV-Vis Spectrophotometer after different intervals of time of irradiation. The degradation of ink using a TiO_2 thin film is very evident in Figure 35.

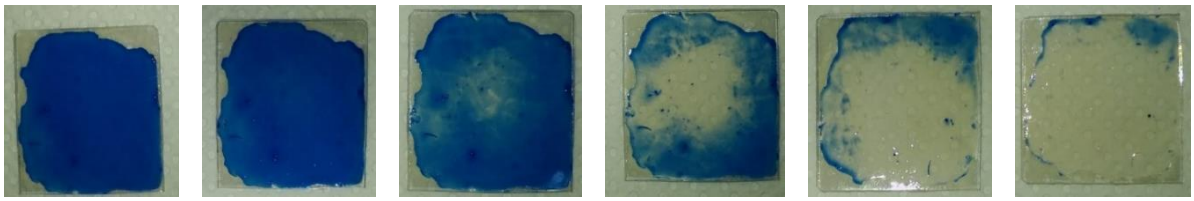

Figure 35 *– Degradation of ink for different intervals of irradiation time in the presence of TiO_2 film as a catalyst.*

The rate of degradation was estimated from the corresponding changes in the peak intensity at 628 nm. Figure 36, Figure 37 and Figure 38 show the variation of absorption intensity for TiO_2, GeZO, and SiZO, respectively. It is possible to observe a decrease in the absorption peak of the ink solution in the presence of all the different semiconductor catalysts.

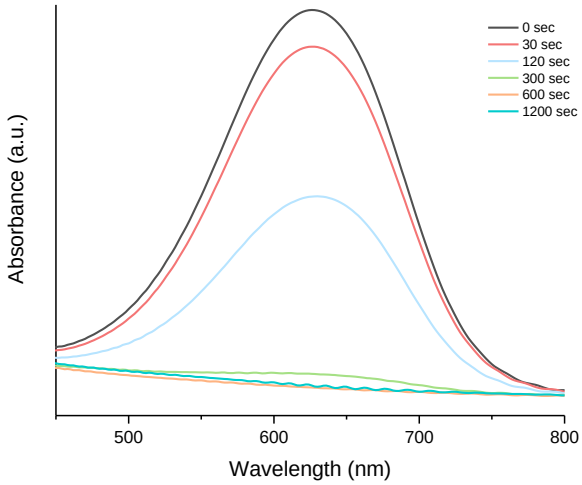

Figure 36 *– The variation in absorption spectra of ink solution as a function of irradiation time in the presence of TiO_2 film as a catalyst.*

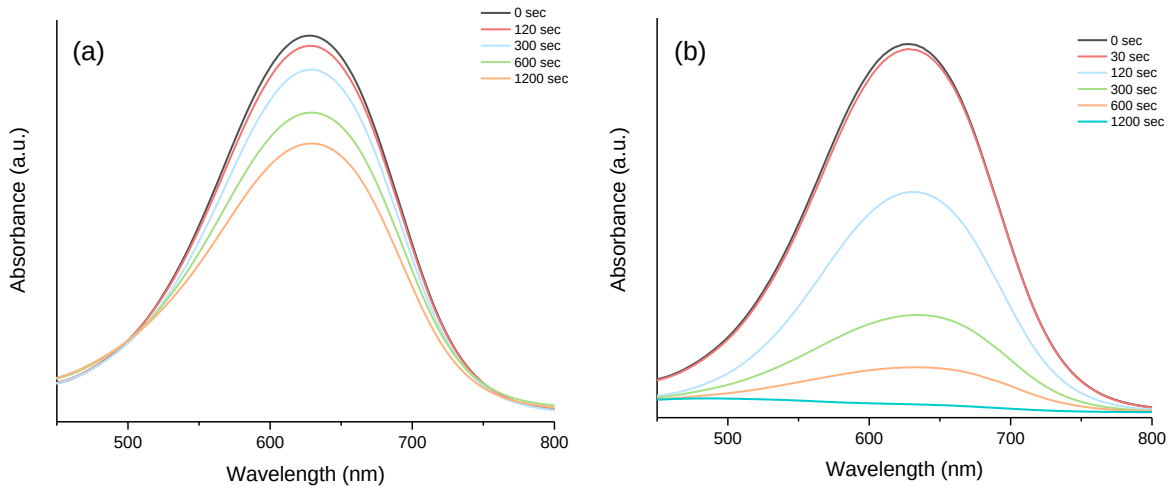

Figure 37 *– The variation in absorption spectra of ink solution as a function of irradiation time in the presence of GeZO as a catalyst. (a) – Sample 2% Ge-I.3; (b) – Sample 2%Ge-II.3.*

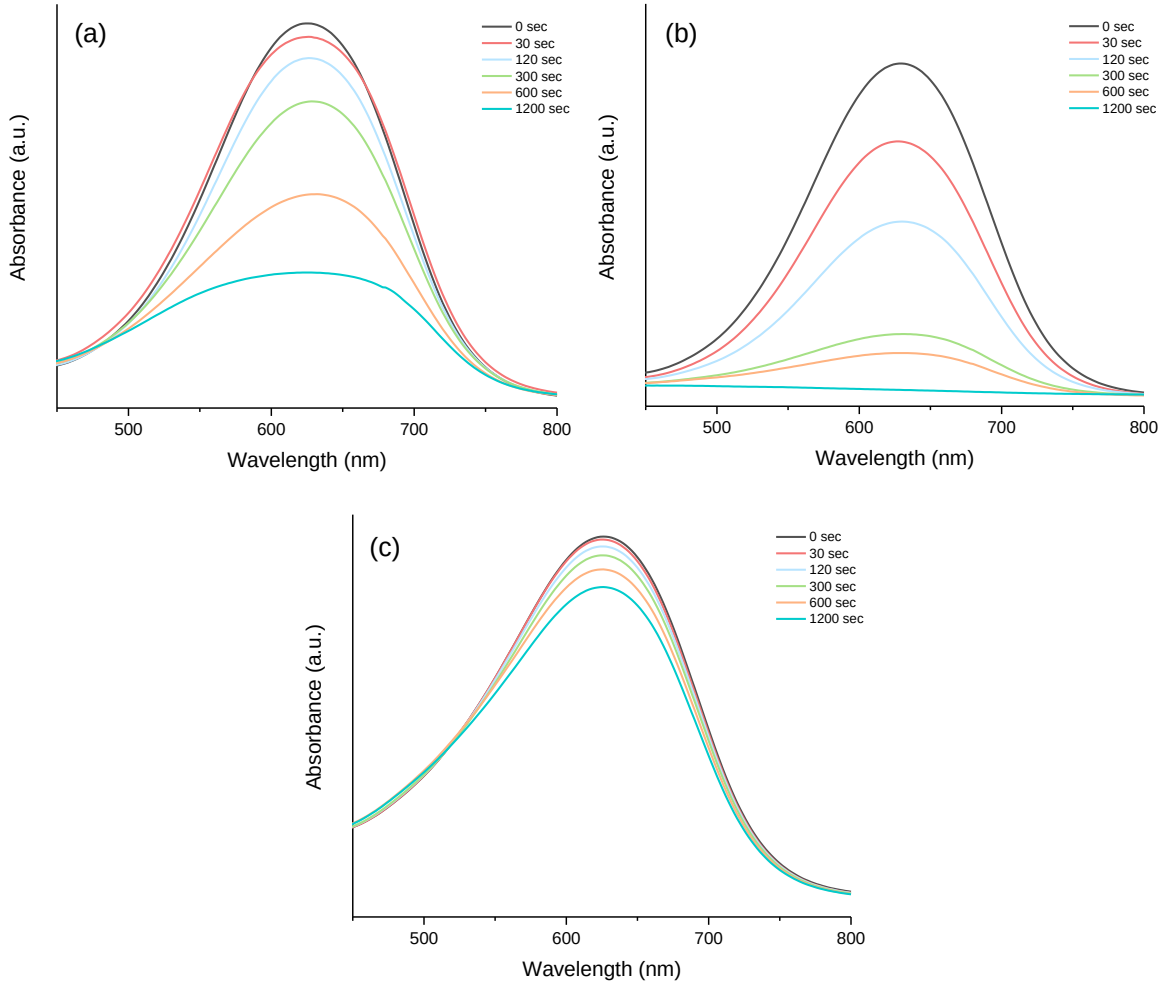

Figure 38 *– The variation in absorption spectra of ink solution as a function of irradiation time in the presence of SiZO as a catalyst. (a) – Sample 1,5% SiZO, 3 layers; (b) – Sample 3% SiZO, 3 layers; (C) – Sample 6% SiZO, 3 layers;*

Figure 39 illustrates the degradation of ink by GeZO thin films and its comparison with uncoated fused silica substrate (control sample) and TiO_2 thin film. As demonstrated by the results, after 1200 seconds, the photocatalytic degradation efficiency follows the order 2% Ge-II.3 > TiO_2 > 2% Ge-I.3 > substrate. The control sample shows a poor photocatalytic activity but can reduce the ink concentration even in the absence of a catalyst. In its turn, in the presence of TiO_2 film, around 90% of initial ink decomposed after 300 seconds (5 minutes). To notice that TiO_2 film reveals a crystallite size of 5,1 nm, a similar value to those obtained for the other films.

GeZO films show a huge difference as a photocatalyst. As described in Table 12, they have a similar crystallite size, and consequently, have a similar surface area, which could be meaning a similar photocatalytic activity due to the higher number of adsorbed molecules of pollutant. Additionally, the obtained values for thickness are close.

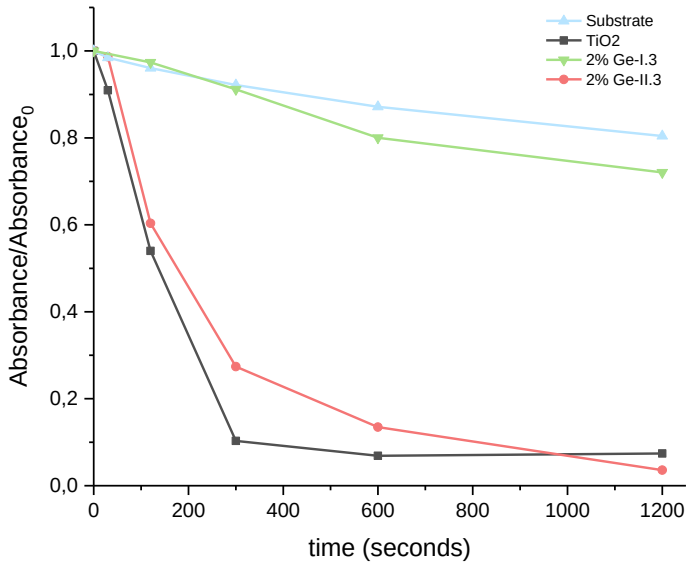

Figure 39 *– Comparison between degradation of blue ink by substrate, TiO_2, and GeZO thin films.*

The degradation of ink by SiZO thin films is observed in Figure 40. The photocatalytic activity increases with the increase of doping to 1.5% for 3% Si but decreases when the doping increases for 6% Si. Indeed, as shown in Table 14, 1.5% SiZO has a higher crystallite size than 3% SiZO and 6% SiZO, which have a similar value. So, increasing the dopant concentration, crystallite size decreases, improving the photocatalytic efficiency. All the samples have a similar thickness.

The 3% SiZO film can degrade about 80% of the initial ink in 300 seconds, only less 10% of the degradation obtained with TiO_2 film.

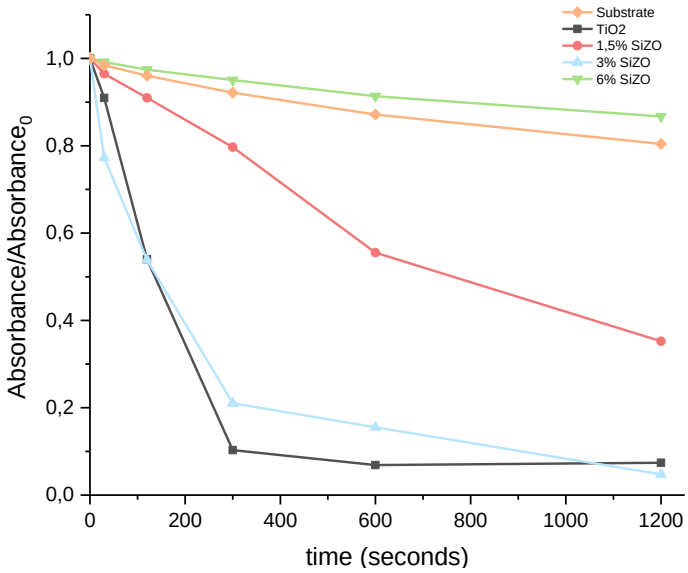

Figure 40 *– Comparison between degradation of blue ink by substrate, TiO_2, and SiZO thin films.*

The line correspondent to TiO_2 film in both graphs suggests a decrease in degraded ink for the last interval of time, which is physically impossible. It is due to the limitations of the procedure. It was used the same UV source with the same intensity in every interval of time. However, it is challenging to put the UV LED to focus on the same spot of the sample without deviation. The same issue happens with the incidence of light in the UV-Vis spectrophotometer. For these reasons, the measurement can be made in a different spot, which contributes to a lower value of degradation.

The differences between both GeZO films and the reduced photocatalytic activity of 6% SiZO compared with the other SiZO films can be related to the amount of ink. Although the ink solution is the same for all samples, its deposited amount can vary for each film, and, therefore, the photocatalytic efficiency will be very different.

To conclude, 2% Ge-II.3 and 3% SiZO thin films have a photocatalytic activity close to TiO_2 film and can be an alternative to degrade pollutants.

5. Conclusions and Future Work

ZnO, Ge-doped ZnO, and Si-doped ZnO thin films were prepared by the Sol-Gel method and the spin coating deposition technique. The effect of Ge and Si dopant on the lattice structure, crystallite size and optical properties of ZnO films was studied.

To understand the influence of several parameters in the ZnO thin film synthesis, the concentration of zinc precursor, the use of different chelating agents, and reaction time were studied. All the parameters promote a good film crystallization, without affecting the lattice parameters. The most concentrated solution guarantees a thickness that does not compromise the electrical properties. However, modifying chelating agents does not introduce any modification in structural properties, and 30 minutes of reaction time is enough to allow ZnO formation.

The development of GeZO thin films by the Sol-Gel approach was not reported yet in literature. It is known that hydrolysis reactions of germanium compounds are very fast in the presence of water, producing turbid solutions, and the use of acetylacetone does not retard them. As-prepared 2% molar GeZO films show an increase in the lattice parameters. However, they should be decreased, due to the smaller radius of Ge atom. The crystallite size exhibits an abrupt reduction when compared with ZnO thin films. Although real doping can not be guaranteed, the introduction of Ge reduces the crystal size improving the photocatalytic activity.

The synthesis of SiZO must be performed with TEOS as a Si-precursor and without the addition of distilled water. Preparing 1.5%, 3%, and 6% molar SiZO films, the lattice parameters and crystallite size decrease with the increase of dopant concentration, due to the replace of Zn atoms for Si atoms in the lattice. The refractive index also increases for higher concentrations of doping. The thickness increases with the number of layers, while the refractive index increases with the increase of doping content.

For both GeZO and SiZO films, UV-Vis Spectroscopy does not show a significant absorption edge, which could compromise the increase of optical properties. However, this measurement was made with films deposited onto fused silica substrate. The nature of the substrate influenced the structural properties, and consequently, the optical properties.

The 2,6-dichloroindophenol ink was successfully degraded using GeZO and SiZO based photocatalysis process under UV irradiation. GeZO and 3% SiZO exhibit an efficiency very close to TiO_2, a well-known semiconductor catalyst. The improvement in photocatalytic activity is suggested to be due to the reduction of recombination rate and the increased surface area of the nanocrystallites.

In future work, GeZO must be synthesized with different Ge concentrations, using a glove box to control the air moisture and to reduce the hydrolysis rate. Another possible approach is to find a compound able to retard the hydrolysis, achieving transparent solutions and films. For SiZO thin films, the concentration of doping must be increased to obtain an optimal value to maximize electrical and optical properties. The absorption edge can also be increased with this approach. For both GeZO and SiZO films, the number of layers should be increased to promote an improvement in electrical properties.

Thus, we can not ensure good electrical and optical properties of these films to substitute ITO in its applications.

In photocatalytic further studies, the ink concentration deposited onto the film layer must be measured and controlled to determine the effective efficiency of photocatalysis. All the samples must have the same size to ensure that the thickness of the film ink is the same. Some experiments can be done varying the ink concentration to understand which is the maximum concentration that films can remove in the studied interval of time.

Concluding, the Sol-Gel method is a low-cost technique to synthesize good ZnO and doped-ZnO thin films. The use of low studied elements belonging to Group IV opens a new way to develop different materials with good optoelectronic properties. Moreover, the study performed in this dissertation may redefine the traditional approach to achieve high efficiency of the photocatalytic activity of ZnO.

References

[1] – Transparent Conductive Oxide Thin Films. Materion Technical Paper. Available on https://materion.com/resource-center/technical-papers/thin-films (consulted on august 2019).

[2] – Minami T. Substitution of Transparent conducting oxide thin films for indium tin oxide transparent electrode applications. Thin Solar Films 516 (2008), 1314-1321.

[3] – Liu Y., et al. ZnO-Based Transparent Conductive Thin Films: Doping, Performance, and Processing. Journal of Nanomaterials (2013), 1-9.

[4] – Minami T. Transparent conducting oxide semiconductors for transparent electrodes. Semiconductor Science and Technology 20 (2005), S35-S44.

[5] – Ellmer K., Resistivity of polycrystalline zinc oxide films: current status and physical limit. Journal of Physics D: Applied Physics 34 (2001), 3097-3108.

[6] – Mukhamedshina D., et al. Fabrication and study of sol-gel ZnO films fou use in Si-based heterojunction photovoltaic devices. Modern Electronic Materials (2017), 3(4),158-161.

[7] – DSY J., and TA, N. Overview on Transparent Conducting Oxides and State of the Art of Low-cost Doped ZnO Systems. SF J Material Chem. Eng. (2018), 1(1), 1004.

[8] – Afre R., Sharma N., et al. Transparent Conducting Oxide Films for Various Applications: a Review. Rev. Adv. Sci. 53 (2018), 79-89.

[9] – Minami T. New n-Type Transparent Conducting Oxides. MRS Bulletin (2000), 25, 38-44.

[10] – Photocatalytic Thin Film Materials and Applications. Materion Technical Paper. Available on https://materion.com/resource-center/technical-papers/thin-films (consulted on 26 September 2019).

[11] – Stadler A. Transparent Conducting Oxides – An Up-To-Date Overview. Materials (2012), 5, 661-683.

[12] – Bädeker K. Űber die elektrische Leitfähigkeit und die thermielektrische Kraft einiger Schwermetallverbindungen. Ann. Phys. 22 (1907), 327, 749-766.

[13] – Memaster H. US Pat.2,429,420 (1947).

[14] – Hutson A. Piezoelectricity and conductivity in ZnO and CdS. Phys. Rev. Lett. 4 (1960), 505-507.

[15] – Lewis B. G., and Paine D. C. Applications and Processing of Transparent Conducting Oxides. MRS Bulletin (2000), 22-26.

[16] – Dixon S., Scanlon D., et al. n-Type doped transparent conducting binary oxides: an overview. Journal of Materials Chemistry C (2016), 4, 6946-6961.

[17] – Dias A. R. Ligação Química. IST Press, 2 Ed. (2009), 375-381, 390-404.

[18] – Kosyachenko L. A. Solar Cells: Thin-Film Technologies. IntechOpen (2011), 121-125.

[19] – Sturaro M., Synthesis and characterization of transparent conductive oxides for gas sensing, solar control and transparent electrode applications. University of Padova (2015).

[20] – Coutts T. J., Perkins J. D., et al. Transparent Conducting Oxides: Status and Opportunities in Basic Research. National Renewable Energy Laboratory (1999), 1-15.

[21] - Kuznetsov V. L., Vai A. T., et al. Electronic transport in highly conducting Si-doped ZnO thin films prepared by pulsed laser deposition. Applied Physics Letters (2015), 17(23), 232103.

[22] – Carolan D., Doyle H. Size Controlled Synthesis of Germanium Nanocrystals: Effect of Ge Precursor and Hydride Reducing Agent. Journal of Nanomaterials (2015), 1-9.

[23] – Xue S. W., Xiang X., et al. Effects of Ge Doping through Ion Implantation on the structural and optical properties of ZnO thin films prepared by Sol-Gel Technique. International Journal of Modern Physics (2006), 21(31), 5257-5263.

[24] – Yu Y. S., Kim B. H., et al. Optical characteristics of Ge doped ZnO compound. Journal of the European Ceramic Society 24 (2004), 1865-1868.

[25] – Arita M., Yamaguchi M., et al. Electrical and Optical Properties of Germanium-Doped Zinc Oxide Thin Films. Materials Transactions (2004), 45(11), 3180-3183.

[26] – Jiang M., Wang Z., et al. Study of structural and optical properties of Ge doped ZnO films. Thin Solid Films 517 (2009), 6717-6720.

[27] – Chalker P. R., Marshall P. A., et al. Atomic layer deposition of germanium-doped zinc oxide films with tuneable ultraviolet emission. J. Mater. Chem. 22 (2012), 12824-12829.

[28] – Kim D. J., Lee M. H., et al. Effect of Oxygen Pressure on Electrical Properties of Ge-doped ZnO Thin Films Grown by Using Pulsed Laser Deposition. J. of the Korean Physical Society (2012), 61(6), 920-923.

[29] – Gaspera E., Duffy N.W., et al. Plasmonic Ge-doped ZnO nanocrystals. Chemical Communications (2015), 51(62), 12369-12372.

[30] – Zhu W., Kammuri T., et al. Structure and composition evaluation of heavily Ge-doped ZnO nanocrystal films. J. Phys. D: Appl. Phys (2018), 51(8), 085302.

[31] – Minami T., Sato H., et al. Highly Conductive and Transparent Silicon Doped Zinc Oxide Thin Films Prepared by RF Magnetron Sputtering. Japanese Journal of Applied Physics (1986). 25(9), L776-L779.

[32] – Qin H., Liu H. F., et al. Si doped ZnO thin films for transparent conducting oxides. Surface Engineering (2013). 29(1), 70-76.

[33] – Das A. K., Misra P., et al. Effect of Si doping on electrical and optical properties of ZnO thin films grown by sequential pulsed laser deposition. J. Phys. D: Appl. Phys. 42 (2009), 165405.

[34] – Clatot J., Campet G., et al. Low temperature Si doped ZnO thin films for transparent conducting oxides. Solar Energy Materials & Solar Cells 95 (2011), 2357-2362.

[35] – Rashidi N., Vai A. T., et al. Origins of Conductivity Improvement in Fluoride-Enhanced Silicon Doping of ZnO Films. Chemical Communication (2015), 51(45), 9280-9283.

[36] – Rashidi N., Kuznetsov V. L., et al. Highly conducting and optically transparent Si-doped ZnO thin films prepared by spray pyrolysis. J. Mater. Chem. C (2013), 1(42), 6960

[37] – Islam M. R., Rahman M., et al. Structural, optical and photocatalysis properties of sol-gel deposited Al doped ZnO thin films. Surfaces and Interfaces 16 (2019), 120-126.

[38] – Photocatalytic Thin Film Materials and Applications. Materion Technical Paper. Available on https://materion.com/resource-center/technical-papers/thin-films (consulted on 26 September 2019).

[39] – Lee K. M., Lai C. W., et al. Recent developments of zinc oxide based photocatalyst in water treatment technology: A review. Water Research 88 (2016), 428-448.

[40] – Hoffmann M. R., Martin S. T., et al. Environmental Applications of Semiconductor Photocatalysis. Chem. Rev. (1995), 95, 69-96.

[41] – Margan P., Haghighi M. Hydrothermal-assisted sol-gel synthesis of Cd-doped TiO_2 nanophotocatalyst for removal of acid orange from wastewater. J. Sol-Gel Sci Technol. (2016), 81(2), 556-569.

[42] – Gnanaprakasam A., et. al. Influencing Parameters in the Photocatalytic Degradation of Organic Effluent via Nanometal Oxide Catalyst: A Review. Indian Journal of Materials Science (2015), 1-16.

[43] – Gaya U. I. Heterogeneous Photocatalysis Using Inorganic Semiconductor Solids. Springer (2014), 92-99.

[44] – Rissman, J, Kennan, H. Low-Emissivity Windows, Case Studies on the Government's role in Energy Technology Innovation, American Energy Innovation Council, 2013.

[45] – Dey A. Semiconductor metal oxide gas sensor: A review. Material Science & Engineering B 229 (2018), 206-217.

[46] – Steinhauser J. Low pressure chemical vapor deposited zinc oxide for silicon thin film solar cells. Lulu.com. ISBN 9781409284512 (2009), 38.

[47] – Tsay C., Fan K., et al. Transparent semiconductor zinc oxide thin films deposited on glass substrates by sol-gel process. Ceramics International 36 (2010), 1791-1795.

[48] – Laurenti M., Cauda V. Porous Zinc Oxide Thin Films: Synthesis Approaches and Applications. Coatings (2018), 8, 67.

[49] – Shakti N., Gupta P. S. Structural and Optical Properties of Sol-gel Prepared ZnO Thin Films. Applied Physics Research (2010), 2(1), 19-28.

[50] – Bahuguna G., Mishra N., et al. Thin Film Coating through Sol-Gel Technique. Research Journal of Chemical Sciences (2016), 6(7), 65-72.

[51] – Znaidi L. Sol-gel-deposited ZnO thin films: A review. Materials Science and Engineering B 174 (2010), 18-30.

[52] – Brinker C. J., Scherer G. W. Sol-gel Science: The Physics and Chemistry of Sol-gel Processing. Academic Press (1990), 13, 787.

[53] – Esposito S. “Traditional” Sol-Gel Chemistry as a Powerful Tool for the Preparation of Supported Metal and Metal Oxide Catalysis. Materials (2019), 12(4), 668-693.

[54] – Livage J., Ganguli D. So-gel electrochromic coatings and devices: A review. Solar Energy Materials & Solar Cells 68 (2001), 365-381.

[55] – Guglielmi M., Carturan G. Precursors for Sol-Gel Preparations. Journal of Non-Crystalline Solids 100 (1988), 16-30.

[56] – Armaleao L., Fabrizio M., et al. Sol-gel synthesis and characterisation of ZnO-based nanosystems. Thin Solid Films 394 (2001), 90-96.

[57] – Hu M. Z., Payzant E. A., et al. Sol-Gel and Ultrafine Particle Formation via Dielectric Tuning of Inorganic Salt-Alcohol-Water Solutions. Journal of Colloid and Interface Science 222 (2000), 20-36.

[58] – Mahmood A., Naeem A. Recent Applications in Sol-Gel Synthesis. IntechOpen (2017), 9, 170-193.

[59] – Sahu N., Parija B., et al. Fundamental understanding and modeling of spin coating process: A review. Indian J. Phys. 83 (2009), 4, 493-502.

[60] – Tyona M. D. A theoretical study on spin coating technique. Advances in Materials Research (2013), 2(4), 195-208.

[61] – Brinker C. J., Hurd A. J., et al. Review of sol-gel thin film formation. Journal of Non-crystalline Solids 147,148 (1992), 424-436.

[62] – Raoufi D., Raoufi T. The effect of heat treatment on the physical properties of sol-gel derived ZnO thin films. Applied Surface Science 255 (2009), 5812-5817.

[63] – Maia A., Ochoa M., et al. Nanocrystalline ZnO thin films – influence of sol-gel conditions on the underlying chemistry and film microstructure and transparency. Materials Today: Proceedings 2 (2015), 49-56.

[64]- Liu Z., Jin Z., et al. Preparation of ZnO porous thin films by sol-gel method using PEG template. Materials Letters 59 (2005), 3620-3625.

[65] – Habiti M. H., Sardashti M. K. Preparation and proposed mechanism of ZnO Nanostructure Thin Film on Glass with Highest c-axis Orientation. International Journal of Nanoscience and Nanotechnology (2008), 13-16.

[66] – Gaspera E. Nobel Metal/Metal Oxide nanocomposite thin films for optical gas sensors. PhD thesis. University of Padova (2011).

[67] – Sorar I., et. al. Optical and structural properties of Si-doped ZnO thin films. Applied Surface Science 257 (2011), 7343-7349.

[68] – Kandpal K., Singh J., t al. Effect of thickness on the properties of ZnO thin films prepared by reactive RF sputtering. Journal of Materials Science: Materials in Electronics (2018), 29(17), 14501–14507.

[69] – W. L. Bond. Measurement of the refractive indices of several crystals, *J. Appl. Phys* (1965), 36, 1674-1677.

[70] – Nagayasamy N., et. al. The Effect of ZnO Thin Film and its Structural and Optical Properties Prepared by Sol-Gel Spin Coating Method. Open Journal of Metal (2013), 3, 8-11.

[71] – Ohyama, M., Kouzuka, H., & Yoko, T. Sol-gel preparation of ZnO films with extremely preferred orientation along (002) plane from zinc acetate solution. Thin Solid Films (1997), 306(1), 78–85.

[72] – Winer I., ShterG. E., et al. Effect of solvents and stabilizers on sol-gel deposition of Ga-doped zinc oxide TCO films. Journal of Materials Research (2011), 26(10), 1309–1315.

[73] – Kayani Z.N., et al. Optical and structural properties of thin films of ZnO at elevated Temperature. Journal of Alloys and Compounds 606 (2014), 177-181.

[74] – Krishnan V., Gross S., et al. Structural Investigations on the Hydrolysis and Condensation Behavior of Pure and Chemically Modified Alkoxides. 2. Germanium Alkoxides. J. Phys. Chem. B (2007), 111, 7519-7528.

[75] – Bonifacio L. D., Lotsch B. V., et al. Periodic Mesoporous Materials: Holes Filled with Opportunities. Comprehensive Nanoscience and Technology (2011), 5.04, 69-105.

[76] – Kamarudiin S., Sahdan M., et. al. Influences of preheating temperature on the structural and optical properties of ZnO thin films by so-gel spin coating technique. Advanced Materials Research 925 (2014), 401-405.

[77] – Lou X., Shen H., et. al. Optical properties of nanosized ZnO films prepared by sol-gel process. Trans. Nonferrous Met. Soc. China 17 (2007), 814-817.

[78] – Xie G.C., Fang L., et. al. Effect of In-doping on the optical constants of ZnO thin films. Physics Procedia 32 (2012), 651-657.

[79] – Kozuka H. Stress Evolution and Cracking in Sol-Gel Derived Thin Films. Springer (2016).

[80] – Zulkifli Z., Sharma S., et. al. Effect on annealing in hydrogen atmosphere on ZnO films for field emission display. IOP Conf. Series: Mat. Science and Engineering (2015), 99, 012030.

[81] – Sabeeh S. H., Jassam R. H. The effect of annealing temperature and Al dopant on characterization of ZnO thin films prepared by sol-gel method. Results in Physics 10 (2018), 212-216.

[82] – Kansal S. K, Chopra M. Photocatalytic Degradation of 2,6-Dichlorophenol in Aqueous Phase Using Titania as a Photocatalyst. Engineering (2012), 4, 416-420.

Appendix A – Instrumentation

A.1 X-Ray Diffraction

An XRD analysis was made to characterize crystalline phases of thin films. A Philips PW1710 diffractometer was used with CuKα filtered radiation at 40 kV and 40 mA. The X-Ray incident angle was set equal to 1°.

A.2 Spectroscopic Ellipsometry

Ellipsometry quantities Ψ and Δ have been measured using a J.A Woollam V-VASE Spectroscopic Ellipsometer in 300-1200 nm wavelength range, using different light angles of incidence (65º, 70º and 75º). Fitting the experimental data of Ψ and Δ with the Cauchy Model, it is possible to obtain the refractive index (n), exciton coefficient (k), and the film thickness.

The Cauchy dispersion relationship is a polynomial and empirical model to transparent materials over specific wavelengths. In this case, k is zero and it is only necessary to fit n, according to equation (*I*).

$$n(\lambda) = A + \frac{B}{\lambda^2} + \frac{C}{\lambda^4} \quad \text{(I)}$$

When the wavelength gets a really high value, the B and C terms tend to zero and, consequently, the refractive index is a constant, equal to A parameter. Indeed, moving from the visible region to the IR, n is a horizontal line. Contrarily, when the wavelength tends to zero, B and C terms tend to infinite and n is infinitely big. However, due to material absorption, there are physical limits that do not allow n to decrease or increase randomly.

To notice that A and B terms are enough to describe the behavior, so C can be zero or ignored.

A.3 Four-Probe Measurement

The Sheet Resistance was measured using a Keithley 2400 Four-Probe equipment. The Four-Probe consists of four electrical probes in a line, equally spaced between each, which measures the Sheet Resistance on the top of the sample. A current (I) is applied into probe 1 and collected through probe 4, while the resultant voltage drop (V) is measured between probes 2 and 3.

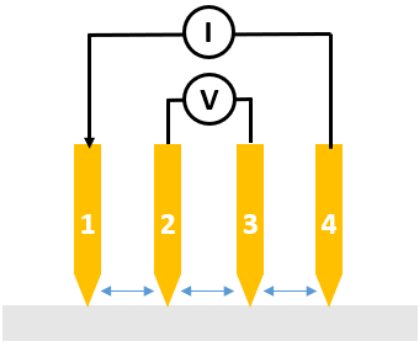

***Figure I** – Schematic representation of the Four Probe technique.*

The Sheet Resistance can be calculated using equation (II).

$$R_S\,(\Omega/sq) = \frac{\pi}{\ln 2} \cdot \frac{\Delta V}{I} \qquad \text{(II)}$$

A.4 Optical Spectroscopy

UV-Vis-NIR Absorption spectra were taken using a Cary 5000 spectrometer. Absorption measurements of thin films deposited on fused silica were analyzed placing the substrate perpendicularly to the light beam.

FTIR measurements have been performed using a JASCO FTIR 6300 instrument, using a resolution of 4 cm^{-1} on films deposited onto a silicon substrate.

The photocatalytic analysis was made using UV-Vis JASCO V-650 spectrometer in range of 200-800 nm.

Appendix B – EDS GeZO analysis

Table I – EDS obtained results of 2% Ge-II.3 thin film.

Element	Apparent Concentration	k Ratio	Wt.%	Wt.% Sigma	Standard Label	Factory Standard
O	6,29	0,02117	13,45	0,33	SiO_2	Yes
Si	56,86	0,45053	76,05	0,38	SiO_2	Yes
Zn	6,02	0,06017	9,99	0,27	Zn	Yes
Ge	0,25	0,00245	0,52	0,10	Ge	Yes
Total:			100,00			

Appendix C – Photocatalytic measurement

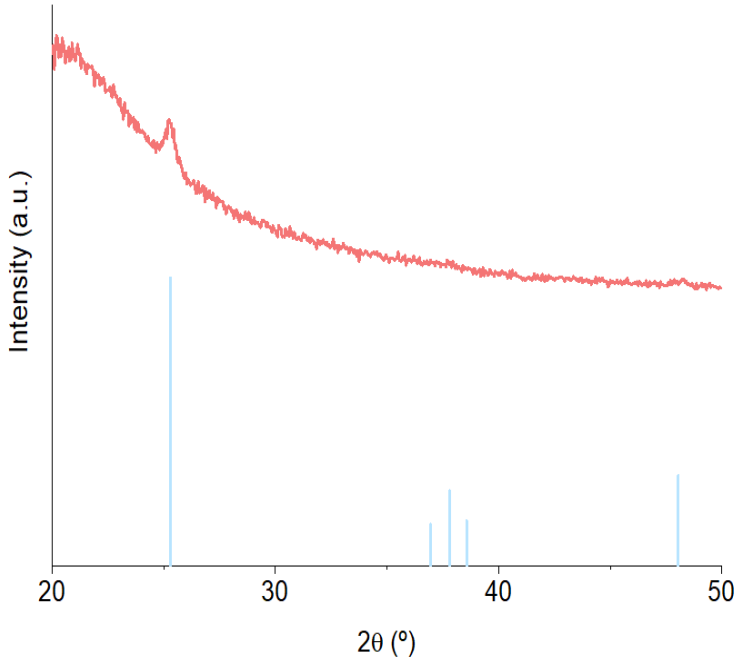

Figure II *– XRD pattern of TiO_2 and corresponding data of JCPDS Nº 84-1285.*